Effect of agitation mode (mechanical, ultrasound and microwave) on uranium sorption using amine- and dithizone-functionalized magnetic chitosan hybrid materials

Khalid Z. Elwakeel [a,b], Mohammed F. Hamza [c,d], Eric Guibal [e,*]

[a] *University of Jeddah, College of Science, Department of Chemistry, Jeddah, Saudi Arabia*
[b] *Environmental Science Department, Faculty of Science, Port-Said University, Port-Said, Egypt*
[c] *Guangxi Key Laboratory of Processing for Non-ferrous Metals and Featured Materials, School of Resources, Environment and Materials, Guangxi University, Nanning [530004], PR China*
[d] *Nuclear Materials Authority, POB530, El-Maadi, Cairo, Egypt*
[e] *Polymers Composites and Hybrids (PCH), IMT Mines Ales, Alès, France*

ABSTRACT

Magnetic chitosan nanoparticles, activated by glycidyl methacrylate, can be functionalized by grafting dieth-ylenetriamine (DETA) and dithizone for improving U(VI) sorption at pH around 5. The physicochemical prop-erties of the materials have been characterized by a wide variety of analytical techniques. Uranyl sorption increases with the pH (progressive deprotonation of amine and sulfur groups). Uptake kinetics are controlled by the agitation mode: the equilibrium time is reduced while using ultrasonic treatment (especially at highest frequency: 80 kHz): the cavitation effect improves the accessibility to internal reactive groups (sorption capacity is increased). The diffusivity coefficient is increased by 4–5 times. In the case of microwave, the sorption capacity is significantly reduced (especially for R-Dithizone, down to 0.8 mmol U g^{-1}) because of temperature increase, which limits the sorption (exothermic mechanism). Mass transfer is tremendously enhanced: equilibrium time is less than 60 s (30 min for ultrasonic treatment and 120 min with mechanical agitation). Sorption capacity at monolayer saturation (Langmuir) decreases with increasing the temperature from 2.20 to 1.74 mmol U g^{-1} for R- Amine (from 1.77 to 1.22 mmol U g^{-1} for R-Dithizone). The sorption enthalpy is close to $-$ 19.7 kJ mol^{-1} for R- Amine (with positive entropy change, $\Delta S°$) and $-$ 34.2 kJ mol^{-1} for R-Dithizone (negative $\Delta S°$). Metal desorption is highly efficient using 0.3 M Na_2CO_3 /0.1 M H_2O_2 solution. Metal desorption is instantaneous (less than 1 min) and complete when using microwave treatment. The ultrasonic treatment allows improving desorption efficiency and decreasing the concentration of the eluent compared with mechanical agitation. The process is successfully applied for uranyl separation from the leachates of marine sediments, especially in the presence of Complexon III (masking agent).

1. Introduction

The exploitation of uranium resources is an important economical and geopolitical challenge for supplying the nuclear power chain. Low-grade ores, as well as tailing wastes, represent alternative resources that are of great interest for obtaining supplementary uranium supplies. Leaching processes allow generating metal-bearing solutions containing a wide range of metals in addition to uranium (base metals, rare earth elements, etc.). The regulations for uranium discharge into the environment are not drastic compared with hazardous metal ions such as Hg (II), Pb(II), Cd(II) or As(V). For example in France, in the course of uranium mine exploitation, the regulations for metal discharge in the water bodies are as high as 1.8 mg U L^{-1}. Provisional guidelines for uranium in drinking water have been set to 30 μg L^{-1} by WHO [1], much higher than the values reported for cadmium (i.e., 3 μg L^{-1}), mercury (i. e., 6 μg L^{-1}), arsenic and lead (i.e., 10 μg L^{-1}). The extraction of uranium from complex solutions may be also of great importance for analytical purpose, although most of the health and environmental risks associated with uranium consist of radiological exposure.

Many techniques may be used for U(VI) removal including

---

* Corresponding author.
  E-mail address: eric.guibal@mines-ales.fr (E. Guibal).

precipitation [2], electrocoagulation [3], reduction-assisted processes [4,5], solvent extraction [6,7], impregnated resins [8], depending on the levels of concentrations and the complexity of the effluent. Sorption properties have retained great attention more specifically for the treatment of dilute solutions using mineral surfaces [9–11], silica [12], functionalized silica [13], biopolymer-silica composite [14], and metal–organic framework [15,16]. Sorption processes using ion-exchange [17–25] and chelating resins [26–28] have been also widely investigated for the treatment of uranium-bearing solutions.

Uranium having a great affinity for amine [29–31], phosphonic [26,32,33] and amidoxime groups [34–36], many resins have been designed by the grafting of these reactive groups on synthetic resins [37] but also on biopolymer-based supports [38,39]. In the current work, magnetic/chitosan nanoparticles decorated with glycidylmethacrylate (GMA) have been functionalized with amine groups (diethylenetriamine, DETA) to prepare GMA-magnetic/chitosan-amine sorbent (R-Amine). The incorporation of magnetic core in sorbent particles allows the readily recovery of micro- or nanoparticles after sorption step. This facility offers the possibility to manufacture very small particles, which, in turn, minimize the contribution of resistance to intraparticle diffusion in the control of global uptake kinetics [30,31,40–42]. The standard support (GMA-magnetic/chitosan NPs) has also been functionalized using dithizone (diphenylthiocarbazone for producing GMA-magnetic/chitosan-dithizone NPs, R-Dithizone) for comparison with R-Amine sorbent. Indeed, dithizone is well known for being a strong complexing agent, which is used in many analytical methods for the detection and quantification of metal ions [43,44]. Dithizone has been also immobilized on many supports for elaborating sorbents applied in metal recovery or analytical procedures: gold [45], silver [46], copper [47,48], mercury [48–50], cadmium [48,51], nickel [48] and uranium [52].

Another objective of this work consists of the evaluation of the impact of agitation mode on uranium sorption performances (both in terms of mass transfer and equilibrium sorption); more specifically the effect of ultrasonic treatment and microwave irradiation are compared with standard mechanical agitation. Recently, ultrasonic treatment has retained great attention for designing fast and efficient sorption processes [17,53–58]; the cavitation effects induced by ultrasonic exposition improve mass transfer properties and accessibility to reactive groups [59–61]. While microwave irradiation has been frequently investigated for activating synthesis procedures [62] or leaching processes [63], both in terms of kinetics and reaction yield, this process has been much less documented for sorption purpose [64–67].

Therefore, the current work compares the sorption performances of two magnetic-chitosan derivatives bearing either DETA or dithizone functional groups. The structure and chemical properties of these materials are characterized using SEM and TEM (morphology), vibrating sample magnetometry (magnetic properties), XRD (crystalline structure based on magnetite), BET analysis (textural characteristics), differential light scattering (DLS, particle size analysis), thermogravimetric analysis, zetametry (surface charge), FTIR spectrometry (chemical characterization of sorbents and metal interactions) and elemental analysis (chemical composition). In a second part of the work, sorption properties are tested through the investigation of pH effect, sorbent dosage, uptake kinetics, sorption isotherms, metal desorption, and sorbent recycling. Special attention is paid to thermodynamic parameters and diffusion properties in relation to the mode of agitation. As an application, the process is tested, under optimized conditions, for the recovery of a series of metal ions (including uranyl) and arsenic from the acidic leachate of sediments collected on Red Sea coast. The effect of Complexon III (used as a masking agent) is evaluated on the sorption efficiency, distribution ratio, and selectivity for uranium uptake with both R-Amine and R-Dithizone materials.

2. Materials and methods

2.1. Materials

All chemicals used were of analytical grade and demineralized water was used for the preparation of all aqueous solutions. Uranyl nitrate hexahydrate ($UO_2(NO_3)_2 \cdot 6H_2O$) was supplied by Sisco Research Laboratories Pvt. Ltd (Maharashtra, India). Glycidyl methacrylate (GMA), diphenylthiocarbazone (Dithizone), epichlorohydrin (chloromethyloxirane), and diethylenetriamine (DETA) were provided by Sigma-Aldrich (Merck, Darmstadt, Germany), while N,N'methylenebisacrylamide (MBA) and benzoyl peroxide (Bz_2O_2) were supplied by Fluka AG (Buchs, Switzerland). Chitosan (deacetylation degree, DA: 87% and molecular weight (in number, MW_n, was 125000 g mol^{-1}) was provided by France Chitine (France). Isopropyl alcohol was provided by Carlo Erba (Barcelona; Spain). Ammonium iron(III) sulfate dodecahydrate ((NH_4)Fe(SO_4)$_2 \cdot 12H_2O$ and iron(II) sulfate ($FeSO_4 \cdot 7H_2O$) were also supplied by Sigma-Aldrich (Merck, Darmstadt, Germany) for the synthesis of Fe_3O_4 nanoparticles.

2.2. Synthesis of sorbents

2.2.1. Synthesis of Fe₃O₄ nanoparticles

Fe_3O_4 nanoparticles were synthesized by the hydrothermal co-precipitation of ferric and ferrous salts according to the method previously reported by Elwakeel et al. [68], derived from Massart [69]. The two precursors (i.e., $FeSO_4 \cdot 7H_2O$, 5.0 g, and (NH_4)Fe(SO_4)$_2 \cdot 12H_2O$, 17.35 g) were dissolved in demineralized water (250 mL). The as-dissolved iron mixture was heated in a conical flask (1.0 L) at 333 ± 1 K, under N_2 atmosphere (provided by nitrogen ballons). The use of nitrogen atmosphere is expected to prevent the fast oxidation of precursor reagents (iron(II), more specifically) and to improve magnetite synthesis. The mixture was magnetically stirred for 60 min. The pH was progressively adjusted to 12 using sodium hydroxide solution (3 M); the reaction continued for 5 h at 318 K. After magnetic separation of the as-prepared Fe_3O_4 particles, the material was repeatedly washed with Milli-Q water (Millipore, Billerica, MA, USA) until the pH of the filtrate became neutral. The solid was finally rinsed with acetone and dried at 333 ± 1 K for 5 h under vacuum. Acetone was used to remove unreacted reagents and to facilitate the drying of the material (by partial solvent exchange).

2.2.2. Synthesis of magnetic chitosan/GMA composite

The first step consists of the preparation of magnetic/chitosan composite using the co-precipitation method. Briefly, chitosan (4 g, powder) was dissolved in a volume of 150 mL of acetic acid solution (10%, w/v). Magnetite precursors (i.e., $FeSO_4 \cdot 7H_2O$, 2.5 g and (NH_4)Fe(SO_4)$_2 \cdot 12H_2O$, 8.67 g) were dissolved in demineralized water (150 mL). Two mL of diluted HCl solution (5%, w/w) were used to boost salt dissolution under continuous stirring for 30 min. After the complete dissolving of iron salts, the solution was mixed with the chitosan solution. Subsequently, the chemical precipitation of magnetic chitosan material was performed at 30 °C under intense stirring by dropwise addition of 20 mL of NaOH solution (50%, v /v) for 30 min, until reaching a pH close to 12. The solid product was recovered by magnetic separation and filtration before being freeze-dried using a freeze-dryer (Bioblock Scientific, Christ) at 223 K and 0.01 mbar; this intermediary product (7.91 g, dry weight) was called MC (magnetic chitosan).

In a second step, the raw resin (Resin R, for magnetic-chitosan-glycidyl-methacrylate macromolecular hybrid material) was prepared by the polymerization of GMA in the presence of MC particles. The mass ratio between GMA and MC was set at 1:1. Therefore, 5.0 g of MC particles were mixed with 5.0 g of GMA in a 500 mL round-bottomed flask equipped with a condenser, then 100 mL of polyvinyl alcohol solution (1%, w/w) was poured into the flask. Three mL of isopropyl alcohol and 25 mL of cyclohexane were then added to the flask under

agitation. Finally, Fe$_3$O$_4$ (1.0 g) nano-particles, the cross-linking agent MBA (0.2 g), and the initiator of the polymerization reaction (0.1 g of Bz$_2$O) were added to the flask. The flask was heated in a water bath at 75–80 °C, under continuous stirring for 3 h. Before being air-dried, the product was washed with demineralized water and acetone. The product was called MCGMA. Scheme 1 describes the preparation of MCGMA

(Resin R). The produced amount of R was 12.32 g (d.w.).

2.2.3. Functionalization of MCGMA – Synthesis of R-Amine and R-Dithizone resins

The raw resin (i.e., MCGMA, R, 12 g) was suspended in 70 mL of isopropyl alcohol. The suspension was reacted with 10 mL of
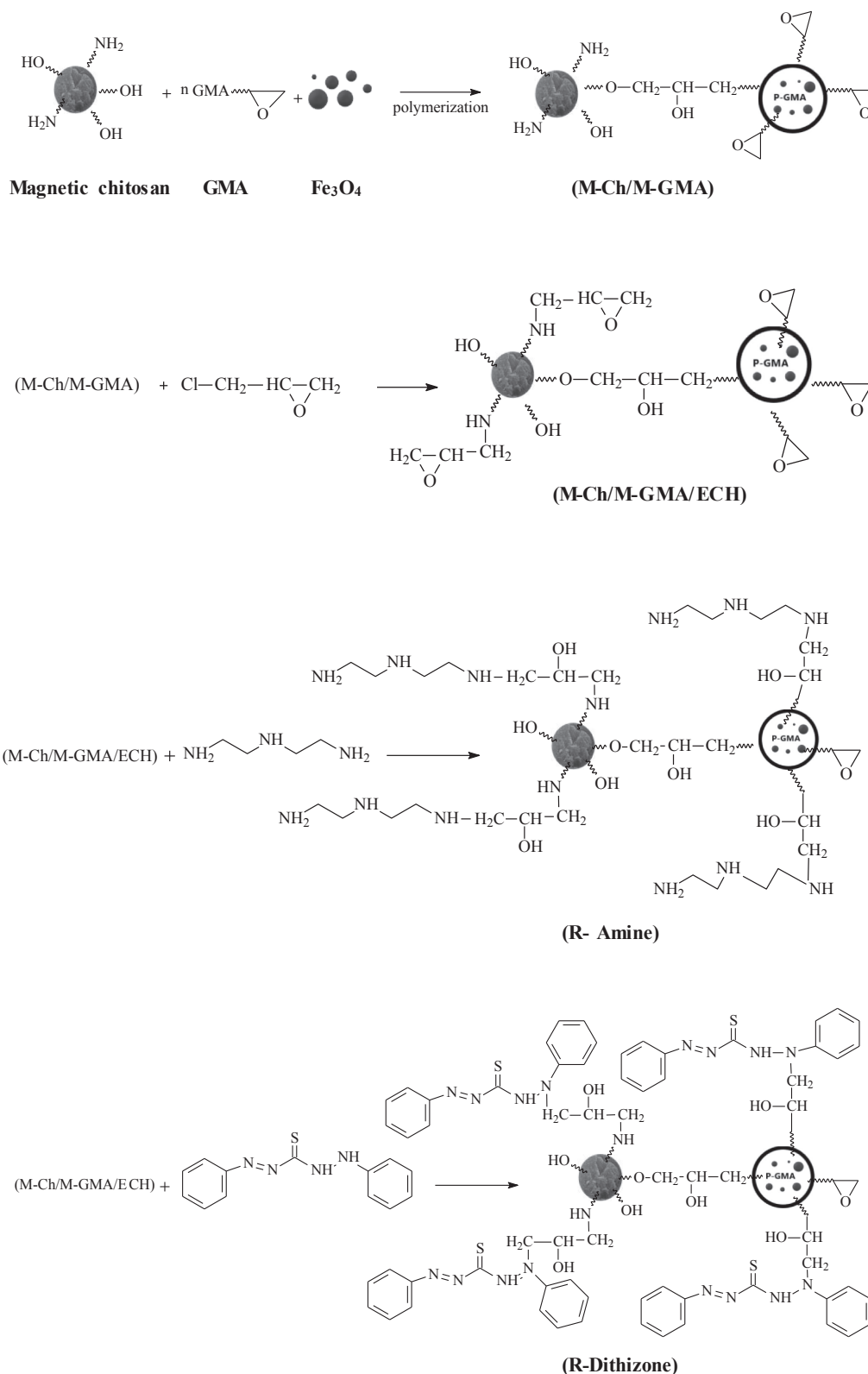
Scheme 1. Synthesis routes for the preparation of R-Amine and R-Dithizone sorbents.

epichlorohydrin (62.5 mmol) dissolved in 100 mL acetone/water mixture (1:1, v/v), under constant agitation at 60 °C for 24 h. The solid was filtered off and washed several times with water (the produced amount was approximately 14.6 g, wet weight). Half the amount of the obtained product was treated with DETA, while the other half was treated with dithizone to produce MCGMA-DETA (herein called R-Amine) or MCGMA-Dithizone (herein called R-Dithizone), respectively. The synthesis procedure consisted of the reaction of (a) 5 mL of DETA (suspended in 100 mL of dioxane) or (b) 1 g of dithizone (in 100 mL of dioxane) with the activated resin (i.e., epichlorohydrine anchored MCGMA). The reaction took place, under agitation, for 12 h at 70 °C. The products were finally air-dried. The produced amounts of resins were 7.55 g and 7.82 g for R-Amine and R-Dithizone, respectively. Scheme 2 reports the suggested structures of the two sorbents.

2.3. Characterization of materials

A Nicolet IS10 FTIR (Thermo Fisher Scientific, Waltham, MA, USA) with an ATR accessory (attenuated total reflectance) was used for FTIR measurements. An element analyzer (PE 2400 II CHN /S, PerkinElmer, Waltham, MA, USA, USA) was used for quantifying the contents of C, H, N, and O in the sorbents. Surface and pore analysis (BET surface, porous volume, and pore size) were performed using a Quantachrome NOVA 3200e (Quantachrome Instruments, Anton Paar Quanta Tec, Inc., Boynton Beach, FL, USA); NovaWin Software (v11.0) was used for data analysis. The size of micro-particles (sorbents and magnetite) was analyzed by differential light scattering using the DLS particle size analyzer NanoBrook 90Plus (Brookhaven Instruments Company, Holtsville, NY, USA). A Shimadzu TGA-50 (Shimadzu Corporation, Tokyo, Japan) was used for thermogravimetric analysis. Sorbent surface charge (zeta potential) were measured using a Nano Zeta Sizer (Nano-ZS Malvern Instruments Ltd., London, UK) at different pH values (from 1.02 to 11.01). Sorbent particles (0.01 g) were suspended in 50 mL of 0.1 M KCl solution for 2 h prior to examination. A vibrating sample magnetometer VSM (PMC MicroMag 3900, Lake Shore Cryotronics, Inc., Westerville, OH, USA) was used for the magnetization tests at room temperature using a maximum 10 kOe magnetic field. The morphology of the studied sorbents was examined with a scanning electron microscope (JSM-6510LV, JEOL Ltd., Tokyo, Japan) before and after binding of uranyl cations. A transmission electron microscope (TEM-2,2100HR, JEOL ltd., Tokyo, Japan) was used for the ultra-high definition characterization of particles suspended in water before being deposited on carbon grids.

2.4. Sorption tests

#### 2.4.1. Sorption and desorption on synthetic solutions
A stock solution (9 mM) of $UO_2(NO_3)_2 \cdot 6H_2O$ was prepared in demineralized water. The working solutions were obtained by dilution of the stock solution with demineralized water just prior to experiments. HNO_3 (0.5 M) and NaOH (0.5 M) solutions were used to control the pH of the solutions. Sorption experiments were performed in batch systems using polyethylene flasks and the temperature was set to 25 ± 1 °C (unless specified).

For the study of pH effect, 20 mL of 3 mM uranium solutions (C_0, mmol U L^{-1}) at different initial pH values (in the range 0.99–6.11) were mixed with 0.02 g of sorbent (d.w.) for 5 h. The stirring speed was maintained at 210 rpm using a shaking incubator (LSI-3016R, Labtech, Sorisole BG, Italy), at room temperature (i.e., 25 ± 1 °C). Samples were collected and the sorbent particles were separated using a magnet; the filtrate was analyzed for residual uranium concentration (C_{eq}, mmol U L^{-1}). The pH was not controlled during the sorption but the initial and final pH values were systematically recorded using a pH meter (HANNA 211, Hanna Instruments, Lingolsheim, France).

For uptake kinetics, 0.2 g of sorbent was mixed with 200 mL of uranium solutions (C_0: 3 mmol U L^{-1}) at initial pH 5.7. The sorbent was magnetically separated at fixed times and the residual concentrations were determined by spectrophotometry using the Arsenazo-III method [70] (collected sample volume was 1 mL). For mechanical sorption, the agitation speed was set at 210 rpm, while the temperature was maintained at 25 ± 1 °C. In order to investigate the influence of ultrasonic or microwave treatments on the sorption of uranyl ions, the sorption experiments were conducted under the same conditions. The unique difference consisted of using an ultrasonic bath sonicator (Elmasonic P300H ultrasonic bath, continuous mode, with power: 380 W, Elma Schmidbauer GmbH, Singen, Germany) or microwave processor (PELCO BioWave Pro® 2.45 GHz microwave processor; frequency = 2.45 GHz; Power Range; 100–750 W, Ted Pella, Inc., Redding, CA, USA). For ultrasonic treatment (UT), two different frequencies were tested corresponding to frequency F1: 37 kHz, and F2: 80 kHz; the temperature was controlled using a thermostatic box. The sorption capacity at time t ($q_{(t)}$, mmol U g^{-1}) was calculated using the mass balance equation: $q_{eq} = (C_0 - C_{eq}) \times V/m$; where C_0 and $C_{(t)}$ are initial and residual (at time t) U(VI) concentrations (mmol L^{-1}), respectively, and m (g) was the amount of sorbent. The decrement in the volume of the solution (V, L) was taken into account for the application of the mass balance equation.

For sorption isotherms, 0.02 g of the magnetic sorbent (m) were mixed with 20 mL (V) of uranium solutions at different initial concentrations (C_0, ranging between 0.33 and 9.05 mmol U L^{-1}) for 5 h. The pH of the solutions was initially set at 5.7. After magnetic solid/liquid separation, the residual concentration (C_{eq}, mmol U L^{-1}) was determined by spectrophotometry. The sorption capacity (q_{eq}, mmol g^{-1}) was also determined by the mass balance equation. The effects of mechanical agitation, sonication, and microwave exposure on uranyl ions uptake at different concentrations were investigated using the same procedures
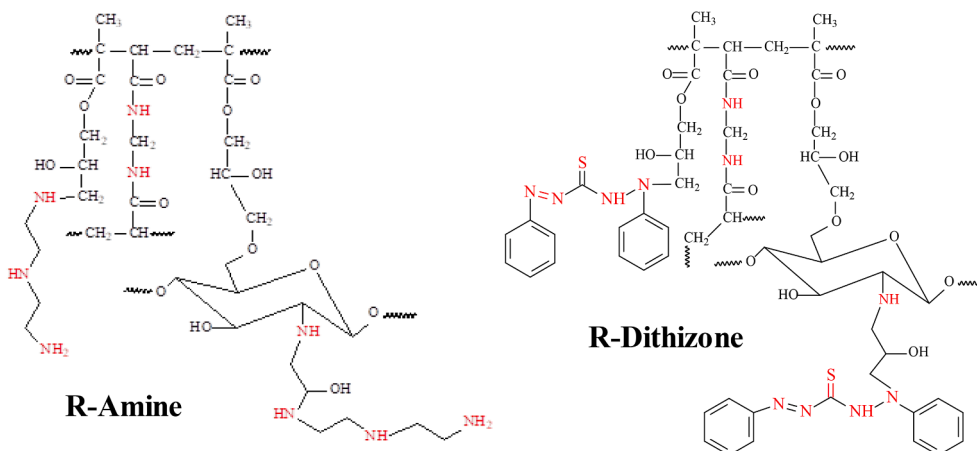
Scheme 2. Suggested chemical structures of R-Amine and R-Dithizone sorbents.

(as above).

For investigating the effect of temperature and thermodynamic studies, sorption isotherms were repeated in shaking incubator (LSI-3016R) at different temperatures, while other experimental conditions were kept the same as described above.

The uptake kinetics and sorption isotherms are modeled using conventional equations summarized in Tables S1a and S1b, respectively. The evaluation of model parameters was performed using non-linear regression analysis (Mathematica ® facilities). The comparison of the different models was based on both the determination coefficients (i.e., R^2) and the AIC values (Akaike Information Criterion, [71]).

For the study of desorption, the sorbent was first loaded by contact of 0.05 g of the sorbent with 50 mL of 9.0 mmol U L^{-1} solution at pH 5.7, at room temperature (i.e. 25 °C). The sorption process was performed using:

(a) mechanical shaking at 210 rpm for 300 min,
(b) ultrasonic treatment (80 kHz) for 50 min, or
(c) microwave treatment (2.45 GHz) for 1 min.

The sorption capacity was determined by the mass balance equation. The solution was magnetically separated and the sorbent was washed with demineralized water. For the desorption step, the loaded sorbent (0.05 g) was mixed with 10 mL of the eluent solution at different concentrations of Na$_2$CO$_3$ (ranging from 0.1 to 0.4 M) mixed with 0.1 M of H$_2$O$_2$. Hydrogen peroxide is supposed to (a) maintain uranium under its highest oxidation state (in case of partial reduction), and (b) facilitate the formation of an extremely stable uranyl peroxo-carbonate complex [72]. The desorption process was performed either in a shaking incubator at 210 rpm, under ultrasound treatment (frequency of 80 kHz) or under microwave treatment (2.45 GHz). Samples were collected at different time intervals and the residual concentrations of uranium were determined by spectrophotometry. The desorption efficiency at time t (DE, %) was calculated according to the following equation:

$$DE(\%) = \frac{\text{Amount of desorbed U (mmol) into the eluate at time t}}{\text{Amount of sorbed U (mmol) at equilibrium}} \times 100 \quad (1)$$

For the study of sorbent recycling; 0.3 Na$_2$CO$_3$ + 0.1 M H$_2$O$_2$ solution mixture was selected as desorbing agent using ultrasound agitation mode (F: 80 kHz) for sorption and desorption, for each sorption/desorption cycles the sorbent particles were collected magnetically, and then carefully washed with ultrapure water for reuse in the next run. Moreover, FT-IR analysis was performed on the sorbent beads at each sorption /desorption cycle in order to detect possible degradation of sorbent particles. Hydrogen peroxide being instable under microwave irradiation, the desorption was performed with simple sodium carbonate solutions.

Uranium was analyzed using Arsenazo-III spectrophotometric method [70]. Briefly, 1 mL uranium(VI) solution sample, 5 mL of chloroacetic acid-sodium acetate buffer solution (pH 2.5) and 1.0 mL of 0.1% aqueous Arsenazo-III solution were mixed in a glass bottle and the final volume of solution was filled up to 25 mL by the addition of demineralized water. The absorbance of the mixture was measured at 660 nm after 10 min of reaction. The measurements were performed by spectrophotometry (T70 + UV/Vis spectrophotometer, PG instruments Ltd, Leicestershire, UK). The analysis of metal ions concentration in the leachate of marine sediment sample was performed using an inductively coupled plasma mass spectrometer (ICP-MS, Elan 9000, Perkin Elmer, Waltham, MA, USA). The concentrations of metal ions (U, Fe, Mn, Cu, Zn, Pb, Ni, Cd, Co, and Hg) and As were analyzed using an inductively coupled plasma mass spectrometer (ICP-MS, Elan 9000, Perkin Elmer, Waltham, MA, USA) [73,74]. The standard curves for U, Cu, Zn, Pb, Ni. Cd, Co, Hg, and As ions were prepared in the concentration range 0–100 μg L^{-1}, while for Fe and Mn the concentrations ranged between 0 and 100 mg L^{-1}. The coefficients of determination (R^2) for all standard curves were higher than 0.997.

Note: all experiments have been triplicated and the plotted data correspond to average values. Annex (see Supplementary Information)

comments on the reproducibility issues (illustrated by some examples on sorption isotherms).

2.4.2. Leaching of marine sediments and metal sorption

Marine sediment sample was collected from the coastal area at Jeddah (Red Sea, Saudi Arabia). The sample was air dried, manually cleaned from extraneous materials (such as snail and crustacean shells). Then the sample was grinded. A 200 g sample was digested with four acids beginning with 20 mL hydrofluoric acid (50%, v/v), followed by 20 mL of a mixture of nitric acid (50%, v/v) and perchloric acids (50%, v/v), then heated using hot plate at 70 °C under fume hood to dryness. Dried samples were finally dissolved into 100 mL of hydrochloric acid (50%, v/v) for 3 days. After this digestion step, the samples were filtered, the pH of the filtrate was adjusted using NaOH to 5.7; the concentrations of metal ions (U, Fe, Mn, Cu, Zn, Pb, Ni, Cd, Co, and Hg) and As were analyzed using ICP-MS. The concentration of chloride ions (485 mg L^{-1}) was determined using Volhard's titration method [75].

Uranium sorption from the pregnant leaching liquor (PLL), containing Fe, Mn, Cu, Zn, Pb. Ni, Cd, Co, Hg and As, was tested using the studied sorbents in a batch reactor, using sonication at 80 kHz frequency for agitation. Experimental conditions were set to pH$_0$: 5.7 (pH$_{eq}$: 5.83); SD: 1 g L^{-1}; T: 25 ± 1 °C; contact time: 50 min. The residual concentrations of metal ions (U, Fe, Mn, Cu, Zn, Pb. Ni. Cd, Co, and Hg) and As were analyzed using ICP-MS.

In order to change the selectivity of the sorbents for target metals, the sorption tests were directly performed on the PLL, but also after adding Complexon III (i.e., disodium salt-EDTA, C$_{10}$H$_{14}$N$_2$Na$_2$O$_8$·2H$_2$O), at the concentration of 0.5 M [76].

3. Results and discussion

3.1. Characterization of sorbents

3.1.1. Physical characteristics

The comparison of SEM pictures for R-Amine and R-Dithizone (materials before and after uranium sorption) shows some differences in the morphology of the sorbents (Figure S1, see Supplementary Information). Both of them are characterized by irregular surfaces: the combination of micro-spherical objects, plane plates, and aggregates. In the case of R-Amine, the granular micro-objects are of smaller size (~50 nm) compared with the globular objects appearing on R-Dithizone (i.e., ~ 50 nm). It is also possible to identify the stacking of "melted" layers; this general structure is completed by aggregated objects. For R-Dithizone, some strands are also observed as linkages between different objects and polymer layers, in addition to globular surface beads. Although the composite (magnetic chitosan-GMA, MGMA-Chitosan) is the same support for the two sorbents, the final surface appears to be affected by the post-functionalization. These irregular surfaces allow anticipating that the sorbents may have a non-negligible specific surface area (see below). It is noteworthy that metal sorption hardly changes the morphology and surface texture of the sorbents.

Figure S2 shows the TEM pictures of the two materials before and after U(VI) sorption. The dense particles (dark objects) embedded in light materials (polymer matrix) represent magnetite particles. SEM and TEM figures show irregular surfaces that allow anticipating that the sorbents have a good specific surface area that makes them suitable for sorption. Similar surface structures have been observed by Kloster et al. [77]. They showed that the surface of the nanocomposite film (chitosan-coated nano-iron oxide particles) is much more irregular (i.e., enhanced surface area) than that of free chitosan film. The SEM images of xanthate-modified cross-linked magnetic chitosan/poly(vinyl alcohol) particles (XCMCP) surface exhibited a microporous and irregular structure comparable with the current sorbents [78]. Surprisingly, the shape and size of these objects depend on the sorbent. For R-Amine, magnetite particles show irregular shapes with particles sizes in the range 8–19 nm, the same shapes are observed with particles sizes in the

range 6–13 nm. In the case of R-Dithizone, two types of objects can be observed: small irregular particles (a few nm, less than 10) and spherical structures (ranging between 40 and 120 nm). After U(VI) sorption, the globular objects apparently disappear and the magnetite particles appear as irregular nano objects (size: 5–12 nm, with some aggregates of larger size, i.e., ~ 30 nm). These differences are unexpected since the support (i.e., magnetite-embedded chitosan functionalized with GMA) is supposed to be the same for R-Amine and R-Dithizone.

The textural properties of the two sorbents are summarized in Figure S3. The two materials show very similar N_2 sorption and desorption isotherms, which are classified as Type IV isotherms according to IUPAC nomenclature. The BET surface (SSA_{BET}) is weakly affected by the type of functionalization: ~ 11 m^2 g^{-1} for R-Amine vs. 9.5 m^2 g^{-1} for R-Dithizone. The pore volumes are close to 0.2 cm^3 g^{-1} and the pore radius varies from 7.5 for R-Amine to 6.3 for R-Dithizone. In the case of magnetic-chitosan microparticles functionalized with tetraethylenepentamine (via methyl acrylate), Zhang et al. [79] obtained a sorbent with a specific surface area close to 6.1 m^2 g^{-1}, pore diameter ~ 6.5 nm, and pore volume ~ 0.015 cm^3 g^{-1} (2.3 m^2 g^{-1}, ~ 12.1 nm and ~ 0.008 cm^3 g^{-1}, respectively, for magnetic chitosan microparticles, prior to functionalization). R-Amine and R-Dithizone exhibit higher SSA_{BET}, higher pore volume and lower pore size. It is noteworthy that these values are one order of magnitude lower than the SSA_{BET} reported by Freire et al. [80] for magnetic chitosan. In their process, the synthesis of magnetite nanoparticles (in the presence of chitosan) was enhanced by sonication.

The X-ray diffraction patterns are reported in Figure S4. MCGMA, R-Amine, and R-Dithizone are presenting very close profiles that are characterized by the peaks at 2θ = 35.4° (3 1 1), 43.1° (4 0 0), 53.1° (4 2 2), which have been associated with Fe$_3$O$_4$ structure [81], the other major peaks at 30.0° (2 2 0), 57.1° (5 1 1), and 62.7° (4 4 0) have been also attributed to magnetite [78,82]. The width of these peaks (with side shoulder at 2θ = 35.4°, for example) is relatively large indicating that the magnetite is effectively present (spinal structure with face-centered lattice and Fd3m space group) but that the material is not perfectly crystalline. Scherrer equation was used for approaching the average size of the crystallites (d,):

$$d = \frac{K \times \lambda}{\beta \times \cos\theta} \tag{2}$$

where K is the grain shape factor (K = 0.94), λ is the incident X-ray wavelength (λ(K_α) = 1.54056 Å), β is the full width at half maximum of the diffraction peak (angle) and θ is the Bragg angle. The crystallite size is evaluated close to 10.6 Å.

The magnetic properties of the sorbents have been analyzed by VSM and compared with non-embedded magnetite particles (Figure S5). The type of modification does not change the saturation magnetization (~19.5 emu g^{-1}); this is about 2.6 times lower than the saturation magnetization of as-prepared magnetite NPs (i.e., 51 emu g^{-1}). The coating of magnetite nanoparticles contributes to reducing the magnetization properties of the material (shielding effect). The second explanation for this decrease in magnetization intensity is the reduced fraction of magnetite into the composite sorbent. The thermal degradation (see below) of the two sorbents showed a residual weight between 14.9% for R-Amine and 10.8% for R-Dithizone; this weight loss is directly correlated to the amount of organic coating. The fraction of magnetite in the sorbent is apparently about 10–15%. Surprisingly, the loss in magnetization (around 64%) is less marked than the effective weight fraction of magnetic NPs in the composite. It is noteworthy that Figure S5 shows that the magnetic-embedded chitosan functionalized with GMA, and MGMA-Chitosan) has an intermediary magnetization behavior between magnetite [83] and functionalized sorbents. However, the curve is much closer to R-Amine and R-Dithizone, showing that the final chemical functionalization has a negligible impact on the magnetic properties compared with the simple coating of magnetite NPs with the GMA-chitosan layers. The coating layer (chitosan

functionalized with glycidylmethacrylate first, followed by amine grafting or dithizone grafting) is constituted of non-magnetic material, which decreases the relative amount of magnetic compartment in the final product (and intermediary product, as shown by the additional analysis of MCGMA). These effects have already been well documented in the literature [78]. This decrease in magnetization is sufficiently limited for making the magnetic nanoparticles readily separable using an external magnetic field. In addition, the absence of a significant hysteresis loop is associated to superparamagnetic behavior. Freire et al. [80] commented that the steep initial slope of the magnetization curve means that the nanoparticles are small enough for considering the NPs as single-domain particles. In their case, the coating of magnetite NPs slightly affected the magnetization of the composite (by 13–22%), consistently with approximate fraction of magnetite in the composite. Actually, the weight loss at 800 °C (measured by TGA) did not exceed 20%. The magnetization saturation is consistent with the levels reported by Dodi et al. [84] (around 51.1 emu g^{-1} for magnetite, 24 emu g^{-1} for magnetic chitosan and 13 emu g^{-1} for functionalized composite).

Differential light scattering may be used for determining the size of sorbent particles: Figure S6 shows the distribution of particles in function of their size for magnetite NPs, R-Amine, and R-Dithizone. Magnetite particles are nanometer-size with an average value close to 31 nm (which is consistent with the order of magnitude of the larger objects embedded in the composites observed in the TEM pictures). On the other hand, the sorbents have a sub-millimeter average size: 0.68 mm for R-Dithizone and 0.78 mm for R-Amine.

3.1.2. Chemical characteristics

The thermal degradation of R-Amine and R-Dithizone is reported in Figure S7 (TGA weight loss and DrTGA curves). The residual weights after complete degradation are close to 11% for R-Dithizone and 15% for R-Amine. The two degradation profiles are relatively close in terms of weight loss vs. temperature. However, the DrTGA curves show substantial differences between the two sorbents. In the case of R-Amine, the main valley appears at 309.4 °C; this is corresponding to the greatest weight variation on the TGA curve. Two additional weak shoulders are detected at 73.9 °C and ~ 470 °C: the first section corresponds to the release of water bound to the polymer, the last one to the degradation of the char (resulting from the degradation of amine groups and the glucose ring of chitosan). In the case of R-Dithizone, similar valleys are identified at 68.1 °C (more marked), 302.4 °C, and ~ 490 °C (more marked); however, the most significant change is identified by the appearance of a new valley at 390.6 °C. The grafting of dithizone on the composite support (magnetic-chitosan functionalized with GMA) introduces a new step in the thermal degradation process (associated with sulfur groups). The weight loss at temperature below 150 °C represents up to 10% (about 3% for R-Amine). This means that in the case of R-Dithizone, water uptake was higher than for R-Amine. The second step in the process is similar for the two sorbents (with a valley for DrTGA in the range 302–310 °C), and corresponds to the degradation of chitosan-based coating: depolymerization of chitosan, degradation of amine groups and epoxide residues. The weight loss is little shifted toward higher temperature for R-Dithizone compared with R-Amine. However, with the new degradation step around 391 °C, the profiles tend to come closer and the final degradation rate is similar (residuals: 11% for R-Amine and 15% for R-Dithizone) at temperatures higher than 560 °C.

Figure S8 shows the FTIR spectrum of magnetic GMA-chitosan support (MCGMA). The large band in the range 3470–3340 cm^{-1} corresponds to the stretching vibrations of –NH and –OH bonds while the peaks and shoulders in the range 3100–2800 cm^{-1} are assigned to –CH/ –CH$_2$ stretching vibrations. The peaks at 1650 cm^{-1} and 1723 cm^{-1} are usually assigned to C = O stretching.

In the case of GMA-bonded polymers (Figure S9), the wide band at 1640–1655 cm^{-1} also includes the contribution of the double-bond of epoxy group [85]. This is a clear marker of the efficient grafting of GMA moiety on chitosan backbone, which is also confirmed by the strong

signal at 1253 cm^{-1} (assigned to epoxy group ring bonds [86]), also identified by the peaks at 841 cm^{-1} [86] and 905 cm^{-1} [87]. A series of peaks corresponding to the carbohydrate ring also appears in the range 1200–900 cm^{-1}. The peak at 580.5 cm^{-1} confirms the presence of magnetite (Fe-O stretching in Fe$_3$O$_4$). Table S2 summarizes the assignment of principal bands with highlights on wavenumber shifts and the appearance/disappearance of peaks associated with the functionalization of the support. The grafting of DETA is followed by (a) the strong decrease in the relative intensities of the epoxy ring vibrations (at 841 cm^{-1} and 905 cm^{-1}), (b) the shift of the characteristic band appearing at 1264 cm^{-1} (instead of 1253 cm^{-1}) and (c) the appearance of a peak at 1573 cm^{-1} (representing N–H stretching vibrations brought by DETA). These changes are consistent with those reported by Wang et al. [88]. In addition, the wide band centered around 1520 cm^{-1} disappears and the two peaks at 1478 cm^{-1} (C-N stretching) and 1449 cm^{-1} (CH$_2$ deformation) are convoluted in a large band centered around 1466 cm^{-1}. These different changes clearly illustrate the efficient grafting of DETA on magnetic-chitosan (through GMA bridging).

The FTIR spectra of MCGMA and R-Dithizone are roughly the same; the main changes concern:

(a) the appearance of a new peak at 691 cm^{-1} (C-S stretching, [89]),
(b) the appearance of a new peak at 1601 cm^{-1} (which may be assigned to different stretching bonds such as: N = N, [48]; N–H [50], which are all present in dithizone),
(c) the refining of the peak at 1526 cm^{-1} (replacing a broad and poorly resolved band at 1520 cm^{-1}), which may indicate the opening of epoxy ring (in GMA).

These changes confirm the immobilization of dithizone on the support through GMA intercalation unit.

The binding of uranyl ions strongly affects the FTIR spectra (Figure S10). For R-Amine, the peak at 1723 cm^{-1} (C = O stretching in carboxylate) is shifted to 1716 cm^{-1}, free carboxyl groups (resulting from epoxy ring opening) may contribute to metal binding; this may be also associated to the pH change resulting from the sorption step at controlled pH. The band at 1567 cm^{-1} (N–H bending) disappears, as the confirmation of the strong contribution of amine groups in metal uptake. The band at 1466 cm^{-1} (C-N stretching) is also considerably decreased, while two new peaks appear at 1422 cm^{-1} and 1343 cm^{-1}. The zone surrounding the band at 1163 cm^{-1} (fingerprint of carbohydrate ring) is also affected by the sorption of uranyl ions.

In the case of R-Dithizone, there is also a shift of the C = O stretching vibration from 1728 cm^{-1} to 1721 cm^{-1}. This means that, in this case again, the possible charge change associated with pH shift (while operating metal sorption) and/or that the carboxyl groups are partly involved in metal uptake. The intensity and the position of some of the R-Dithizone bands are slightly changed. However, the most significant changes may be identified in the range 1370–1315 cm^{-1}, where many small peaks appear (their convolution leads to a poorly resolved zone). The peak at 1257 cm^{-1} is widened with the convoluted spectrum covering at least two poorly-resolved contributions. The 1211–1078 cm^{-1} region is also affected by uranyl sorption: the shoulders at 1184 cm^{-1} and 1132 cm^{-1} are weakened: S = C-N chemical environment is probably affected by uranyl binding. This is confirmed by the splitting of the peak at 1453 cm^{-1} (S = C-N stretching) with an enlargement of the band (and formation of a peak at 1448 cm^{-1}). The other signals at 993 cm^{-1}, 906 cm^{-1}, 845 cm^{-1}, 754 cm^{-1}, and 690 cm^{-1} are also slightly modified (some splits corresponding to the superposition of uranyl nitrate bands). Indeed, the binding of uranyl ions is frequently associated with the appearance of a band at 917–912 cm^{-1} that corresponds to the asymmetric stretching vibration of O = U = O unit [29,90]. Here, this band is "hidden" in the poorly resolved region 970–900 cm^{-1}. A series of small peaks at 745 cm^{-1}, 826 cm^{-1}, 1343 cm^{-1} could be assigned to nitrate ligand attached to bound uranyl (-N-O symmetric bending, -N-O out of plane rocking, -N = O symmetric bending, respectively, [91]).

Uranium sorption proceeds on R-Amine through interactions with amine groups, with the possible contribution of COO– (resulting from residual epoxy ring opening). In the case of R-Dithizone, in addition to these groups, the change in the chemical environment of S = C-N indicates that these reactive groups may also contribute to uranyl binding (probably bound as a nitrate form). Scheme 3 summarizes the tentative mechanisms involved in uranium bending on both R-Amine and R-Dithizone sorbents.

The FTIR spectra were analyzed after each sorption and desorption steps in order to evaluate the chemical stability of the sorbents when recycled five times. Figures S11a and S11b show that the FTIR spectra are remarkably stable while re-using the material. Apparently, the alternative contacts with uranyl solution and eluent do not significantly change the chemical signatures of the materials. The sorbent is readily restored by the eluent (see below).

The elemental analyses of the two sorbents are reported in Table S3. It is noteworthy that the DETA functionalization substantially increases nitrogen (amine) content. In chitosan, the molar N content (which depends on the grade of deacetylation) may be considered close to 5.5 mmol N g^{-1}. Taking into account that about 10–14% of the weight of the sorbent is constituted of magnetite NPs the actual N content may be close to 5 mmol g^{-1}. In magnetic GMA-chitosan, the actual N content is lower (close to 3.14 mmol g^{-1}) due to the weight variation associated with GMA grafting. The analyzed N content is close to 10.0 mmol N g^{-1} for R-Amine. This means that the nitrogen content was increased by about 7 mmol N g^{-1}, which corresponds to almost 2.3 mmol DETA per g of sorbent. This also means that the grafting is highly efficient, amine groups on chitosan backbone being substituted to a yield close to 74%. In the case of R-Dithizone, the S content is close to 1.17 mmol g^{-1}, and the nitrogen content was increased by 4.1 mmol N g^{-1}. The stoichiometric ratio N/S (in terms of load increase) is about ~ 3.5:1, while in the dithizone formula the expected ratio is 5:1. The dual grafting mode (i.e., chitosan/GMA and GMA/Epichlorohydrin interactions with DETA or Dithizone) makes difficult the determination of an accurate grafting yield. In any case, the increases in both N and S element percentages confirm the efficient grafting of reactive groups on the MCGMA support.

Figure S12 shows zetametric measurements for both R-Amine and R-Dithizone. Actually, the two sorbents have comparable acid-base properties. They have a global positive charge in acidic solutions (below pH 7.5) while deprotonation of reactive groups is achieved in alkaline conditions. The decrease in zeta potential is almost linear (with very close values of slope). The pH$_{PZC}$ values deduced from the curves are 7.6 for R-Amine and 7.5 for R-Dithizone. These values are consistent with the data collected in the literature for sorbent grafted with similar reactive groups. In the case of DETA-functionalization of magnetic graphene, Fraga et al. reported pH$_{PZC}$ value close to 8.2 [92], while the functionalization of magnetic Co-imprinted composite with dithizone allowed obtaining a sorbent with a pH$_{PZC}$ close to 7.3 [93]. The protonation of reactive groups may be of great importance for the sorption of uranyl (mainly present as cationic species in acidic solutions, Figure S13).

3.2. Sorption properties

3.2.1. pH effect

The sorption properties may be influenced by the pH (and the composition of the solution: the presence of competitor ions, ligands) through a number of mechanisms or phenomena including:

(a) the metal precipitation (at the highest pH values),
(b) the speciation of the metal; in the case of U(VI), possibility to form polynuclear polyhydrolyzed species, or
(c) the overall charge of the sorbent (protonation/deprotonation of reactive groups).

In the case of uranyl, the precipitation depends not only on the pH
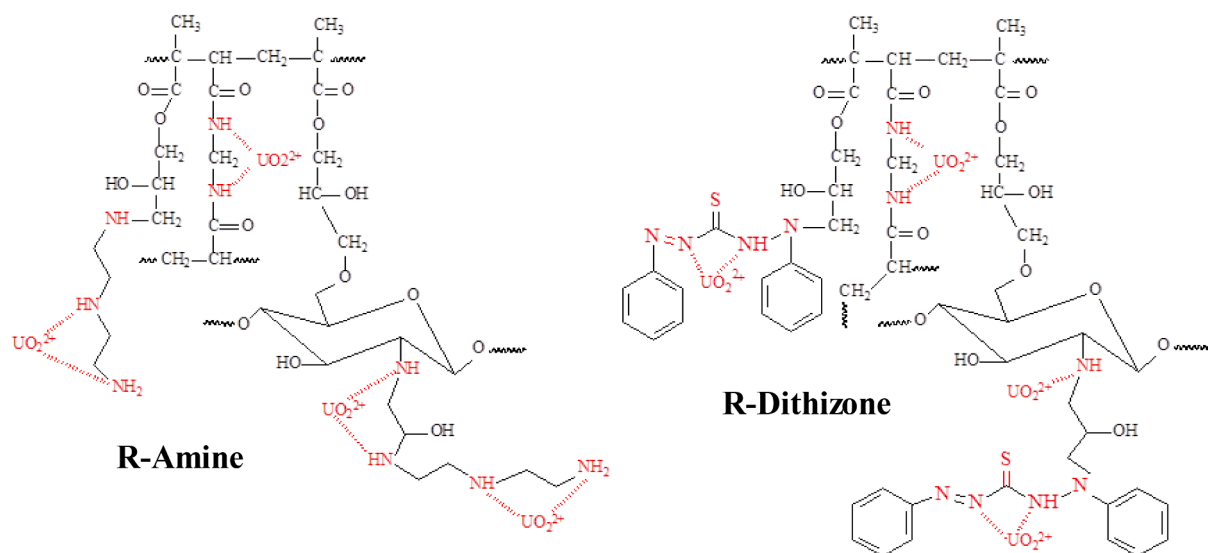
Scheme 3. Tentative mechanisms for the interaction of U(VI) with R-Amine and R-Dithizone.

but also on the total concentration of the metal. The pH_{PZC} of the sorbents being close to 7.5: the reactive groups remain protonated on the whole acidic range of uranyl solubility. Fig. 1 shows the effect of equilibrium pH on the sorption capacity (opened symbols). As expected, increasing the pH progressively increases the sorption capacity for both R-Amine and R-Dithizone sorbents. The progressive decrease of the overall charge of the sorbent enhances the ability of the sorbents to bind uranyl cations. In strong acid solutions, the protonated charges repulse free uranyl and the sorption is negligible (below 0.3 mmol U g^{-1}). When the pH exceeds 5.8, apparently, the sorption capacity steeply increases; this is due to the beginning of the formation of hydrolyzed uranyl species (which, in turn, induces the precipitation of the metal). Fig. 1 also reports the pH variation (initial pH value compared with equilibrium pH). The sorption process is followed by an increase in the pH value by less than 0.3 pH unit (except at pH_0: 3.2 where the pH increases by 0.6 pH unit). As expected, for pH_0 higher than 6, the equilibrium pH tends to decrease due to the precipitation phenomenon.

While elaborating molecularly imprinted polymers based on metaldithizonate templates, Fu et al. [48] showed that the pH influences the formation of the template. In acidic solutions, the metal forms chelate with amine groups of dithizone ketone form while in neutral or alkaline solutions divalent metal cations bind to the dithizone enol form (with contribution of sulfur group). However, this change operates at pH

higher than 5. Therefore, in most cases, it is possible anticipating that the binding mechanism will be mainly controlled by the deprotonation of amine groups and azo bound.

On the other hand, previous studies on uranyl biosorption have highlighted the correlation between the formation of polynuclear species (and progressive deprotonation of amine groups) and the increase in the sorption of U(VI) on *Mucor miehei* fungal biomass (a chitosan-rich fungus) [94]. A similar interpretation may be proposed for explaining the pH effect on uranyl sorption using R-Amine and R-Dithizone sorbents: combined effects of pH on the deprotonation of reactive groups, and formation of polynuclear species. In addition, in the case of R-Dithizone, the partial enolate formation may bring alternative S-based reactive groups for metal binding, at the highest pH values.

Figure S14 plots the distribution ratio (D = q_{eq}/C_{eq}, L g^{-1}), in log_{10} units, *vs.* the equilibrium pH for R-Amine and R-Dithizone sorbents. The plots are roughly linear with slopes close to + 0.408 and + 0.225, respectively. For ion-exchange mechanisms, the slope is usually associated to the stoichiometric ratio of proton/metal exchange. In the present case, the values are poorly compatible with possible stoichiometric ratios; this is consistent with the suggested mechanism of chelation with amine groups (and eventually S groups for R-Dithizone).

3.2.2. Effect of sorbent dosage (SD)

Figure S15 shows the effect of sorbent dosage on the sorption capacity for the two sorbents and the different modes of application. As expected, the increase in the sorbent dosage (SD)(from 0.5 to 5 g L^{-1}) leads to a progressive decrease in the sorption capacity. With the increase of sorbent dosage, the excess of sorbent does not allow optimal use of the highest density of reactive groups and the concentration gradient is less favorable to the saturation of the sorbent. In most cases, the sorption capacity hardly varies between 0.5 and 1 g L^{-1}, drastically decreases from 1 to 3.5 g L^{-1}, and tends to stabilize (slight decrease) above 3.5 g L^{-1}. The agitation mode influences sorption performance according to the series: UT-F2 > UT-F1 > MA ≫ μW. The differences are more marked at low sorbent dosage (below 2 g L^{-1} for R-Amine, below 3.5 g L^{-1} for R-Dithizone) for ultrasonic treatment agitation and mechanical agitation, and the curves merge above these SD limit values. This effect of agitation mode is more marked for R-Dithizone sorbent. It is noteworthy that the decrease (in proportion) with increasing sorbent dosage is much less marked for microwave irradiation than for the other agitation modes: Δ= − 49% *vs.* −68/-72% for R-Amine, and Δ = -45% *vs.* −56/-67% for R-Dithizone.
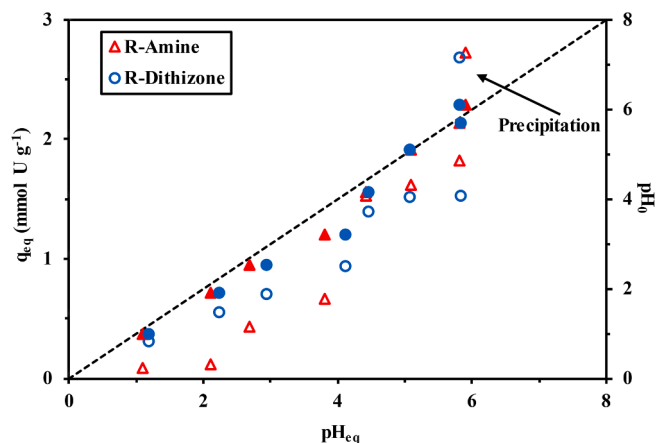

Fig. 1. Effect of pH_{eq} on U(VI) sorption using R-Amine and R-Dithizone sorbents (opened symbols) and pH variation (closed symbols) (C$_0$: 3 mM; Sorbent dosage, SD: 1 g L^{-1}, Contact time: 5 h; T: 25 ± 1 °C; v: 210 rpm).

3.2.3. Uptake kinetics

In sorption processes, the kinetic profiles may be controlled by mass transfer properties (including resistances to bulk diffusion, film diffusion, and intraparticle diffusion), thermal exchanges, as well as the proper reaction rate. In order to evaluate the contribution of these different mechanisms on the uptake kinetics, experiments were performed at different temperatures (in order to calculate activation energy) and with different modes of agitation (mechanical agitation, ultrasonic treatment, and microwave treatment) that are supposed to control mass transfer properties.

3.2.3.1. Effect of temperature on kinetic profiles. Fig. 2 compares the kinetic profiles for U(VI) sorption using R-Amine and R-Dithizone at three temperatures (i.e., 25 °C, 35 °C, and 45 °C). R-Amine sorbent is more efficient than R-Dithizone, regardless of the temperature: equilibrium concentrations being systematically higher when using R-Dithizone under similar experimental conditions. The initial slopes of the kinetic curves are superposed for each individual sorbent: the temperature does not influence the mass transfer within the first 10–15 min of contact (the section where resistance to film diffusion may play the most significant role in the control of mass transfer). In the second section of the curves, the temperature produces a greater effect: increasing the temperature reduces the efficiency of the sorption as shown by higher equilibrium concentrations, for both R-Amine and R-Dithizone. The sorption of U(VI) is an exothermic process.

The three models (pseudo-first order rate equation, PFORE, pseudo-second order rate equation, PSORE, and the resistance to intraparticle diffusion [95], RIDE, or Crank equation [96]) have been systematically compared for the fitting of experimental profiles. The parameters of these models (and the comparative statistical criteria) are summarized in Table 1. In most cases, the highest correlations are obtained with the PSORE (with the exception of R-Amine at 25 °C, where the PFORE gives a little better fit of the kinetic profile). The PSORE is usually associated with chemical bonding while the PFORE is assigned to physical interactions. However, the discussion of kinetic modeling controlling mechanisms has been recently widely debated to highlight the required precautions for getting access to real driving mechanisms [97]. Hubbe et al. [98] pointed out the importance of selecting appropriate experimental conditions (in relation to concentration variation with metal concentration and sorbent dose). They concluded that the PSORE is frequently associated to control of uptake kinetics by resistance to intraparticle diffusion. This is consistent with the current data: the RIDE drives to a much better fit of experimental data than the PFORE (Figures S16 and S17, and Table 1). As expected from Fig. 2, the sorption capacity predicted by the PSORE decreases with increasing the

Table 1
Effect of temperature on U(VI) uptake kinetics under mechanical agitation – Parameters for the PFORE, PSORE and RIDE models.

Model	Parameter	Sorbent R-Amine			R-Dithizone		
	T °C	25	35	45	25	35	45
Exper.	$q_{m,exp.}$ (mmol g^{-1})	1.82	1.77	1.62	1.53	1.38	1.34
PFORE	$q_{eq,1}$ (mmol g^{-1})	1.78	1.67	1.53	1.43	1.31	1.28
	$k_1 \times 10^2$ (min^{-1})	8.00	10.7	11.9	5.60	5.47	5.74
	R^2	0.996	0.972	0.973	0.979	0.986	0.972
	AIC	−161	−129	−134	−135	−146	−135
PSORE	$q_{eq,2}$ (mmol g^{-1})	1.93	1.79	1.63	1.59	1.46	1.42
	$k_2 \times 10^2$ (g mmol^{-1} min^{-1})	6.36	9.83	12.4	4.93	5.17	5.76
	R^2	0.989	0.999	0.999	0.999	0.997	0.997
	AIC	−142	−183	−188	−186	−173	−175
RIDE	$D_e \times 10^9$ (m^2 min^{-1})	1.29	1.56	1.86	0.687	0.762	0.821
	R^2	0.993	0.991	0.989	0.996	0.996	0.995
	AIC	−149	−138	−137	−155	−164	−164

temperature for the two sorbents. However, the comparison of apparent rate coefficients (i.e., k_2) shows different trends for the two materials: k_2 increases with temperature for R-Amine (from 6.36×10^{-2} to 12.4×10^{-2} g mmol^{-1} min^{-1}), while the variation of the material is much less marked in the case of R-Dithizone (in the range 4.93–5.76 $\times 10^{-2}$ g mmol^{-1} min^{-1}). In addition, the apparent rate coefficient is about two times higher for R-Amine than for R-Dithizone at the highest temperature (and of the same order for lower temperature). This means that U(VI) sorption is more sensitive to temperature for R-Amine, the sorption being more depreciated by temperature increase.

The Arrhenius equation was used for calculating the apparent energy of activation (E_a, J mol^{-1}, [99]) using Eq. (3) and the apparent rate coefficients k_2:

$$lnk_2 = -\frac{E_a}{RT} + \ln A \tag{3}$$

Figure S18 shows the plots for R-Amine and R-Dithizone: the energies of activation are relatively low: about 29.6 kJ mol^{-1} and 6.9 kJ mol^{-1}, respectively. The value for R-Dithizone is lower than the value reported by Bai et al. [100] for U(VI) sorption onto alginate beads (∼30 kJ mol^{-1}), which is comparable to the value reached for R-Amine. The order of magnitude of the activation energy has been used for discussing the sorption mechanisms: this order of magnitude is consistent with activated chemical sorption [100].

The effective diffusivity coefficients (D_e) increases with temperature: the temperature slightly improves the Brownian mobility of uranyl ions. The value of D_e for R-Amine is about twice the value for R-Dithizone. Pérez-Conesa et al. [101] reported a value close to 2.94×10^{-7} m^2 min^{-1} for the self-diffusivity of uranyl in water; this is about 3 orders of magnitude higher than the effective diffusivities calculated for the two sorbents. This is another evidence that the resistance to intraparticle diffusion is playing a non-negligible role in the control of uptake kinetics.

The temperature enhances the mass transfer properties and activates the reaction kinetics but negatively influences the thermodynamics of uranyl sorption. This will be confirmed by the study of temperature effect on sorption isotherms (see below).

3.2.3.2. Effect of agitation mode on kinetic profiles. Figure 3 compares the kinetic profiles for U(VI) sorption using R-Amine and R-Dithizone under mechanical agitation (MA), ultrasonic treatment (UT at two frequencies; UT1: 37 kHz and UT2: 80 kHz), and microwave treatment
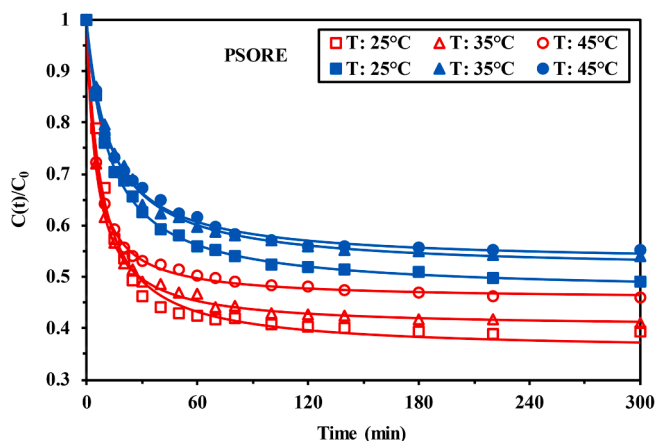

Fig. 2. Effect of temperature on U(VI) uptake kinetics using R-Amine (opened symbols) and R-Dithizone (closed symbols) (pH: 5.7; C_0: 3 mM; Sorbent dosage, SD: 1 g L^{-1}; T: 25 ± 1 °C; v: 210 rpm; solid line: PSORE modeling).

(μW). Table 2 summarizes the parameters of the models used for fitting kinetic profiles. For MA and UT, the figure includes the PSORE simulation (Fig. 3a; Figure S19 for PFORE and Figure S20 for RIDE), while for the very fast kinetics observed with μW, the three models are all presented in Fig. 3b. In most cases, the PSORE fitted better experimental profiles than PFORE and RIDE models (Table 2); the unique exception corresponds to MA with R-Amine sorbent. The comparison of kinetic profiles clearly demonstrates the superiority of ultrasonic treatment on mechanical agitation for the sorption of U(VI) using the two sorbents. This enhancement can be measured on both equilibrium performance and mass transfer. The beneficial effect on sorption capacity increases with the frequency of the UT. R-Amine sorbent is more efficient than R-Dithizone; it is noteworthy that under UT2 agitation conditions, the differences between the two materials are less marked. Strong UT improves the accessibility and availability of reactive groups. While 90–120 min are necessary for reaching equilibrium under MA, the UT only requires 30 min. Similar enhancement of U(VI) uptake kinetics by ultrasonic treatment (with increasing frequency) has been recently reported by Wen et al. [17]. They reported the different mechanisms that may affect sorption process: the cavitation bubbles may locally produce extreme conditions (such as high temperature, high pressure and high speed micro flow; which, in turn, influence the internal diffusion). The case of microwave irradiation is different: μW shows adverse effects on U(VI) sorption: the equilibrium is reached within 60 s of contact (strong enhancement of mass transfer) at the expense of a significant decrease in sorption capacity at equilibrium compared with UT2 treatment and MA agitation. This may be directly connected to the effect of temperature. Indeed, ultrasonic and μW treatments tend to substantially increase the temperature of the solution (especially μW): after 70 min of UT treatment the final temperatures reach up to 35–37 °C for UT1 and 49–52 °C for UT2; however, with μW treatment, the temperature drastically increases to 90–93 °C. The preceding section showed that U(VI) sorption is exothermic and that the uptake kinetics is slightly improved by temperature, while the equilibrium sorption capacity decreases. The trends observed when varying the mode of agitation are consistent with the effect of temperature. This is also consistent with the specific effects of UT treatments and μW irradiation (i.e., sorbent activation and cavitation), which were already demonstrated in the case of synthesis processes assisted by UT and μW.

These trends are confirmed by the comparison of the parameters of the models reported in Table 2. For R-Amine, the equilibrium sorption capacities are increased by 11% and 26% for UT1 and UT2, respectively while the μW treatment strongly reduces the value by 41%. Similar trends are observed for R-Dithizone (i.e., +14%, +50% and − 42%, respectively). On the other side, the apparent rate coefficients k_2 are increased with UT (by 4.3 times) and drastically expanded with μW treatment (83 times) for R-Amine sorbent. For R-Dithizone, the enhancement is even increased (i.e., ×5.8, ×6.5, and × 5133,
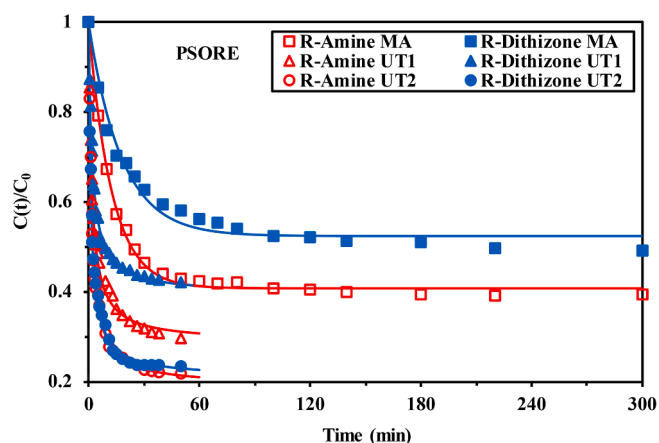

Fig. 3a. Effect of agitation mode on U(VI) uptake kinetics using R-Amine and R-Dithizone sorbents (MA: mechanical agitation – 210 rpm; UT1: ultrasonic treatment 37 kHz; UT2: ultrasonic treatment 80 kHz; pH: 5.7; C_0: 3 mM; Sorbent dosage, SD: 1 g L^{-1}; T: 25 ± 1 °C; solid line: PSORE modeling).

respectively). The enhancement of mass transfer properties in microwave-assisted sorption properties was already reported for the removal of metal ions [102,103] and dyes [64]. Contact times as short as 30–60 s were reported as sufficient for reaching equilibrium [64,103]. Mahmoud et al. [102,103] identified both the effect of increased temperature and diffusion enhancement as the major causes of sorption enhancement.

The effective diffusivities are also increased by a factor 33–3.2 for R-Amine and 6,2–5.4 for R-Dithizone. In this case, the lower frequency for ultrasonic treatment is slightly better than the higher energetic ultrasonic treatment. For microwave irradiation, the effective diffusivities are increased 102 times and 147 times for R-Amine and R-Dithizone, respectively. The microwave-assisted sorption of U(VI) on functionalized sorbents correspond to diffusivities in the range 1–1.3 × 10^{-7} m^2 min^{-1}, which are of the same order of magnitude as the self-diffusivity of U(VI) in water (i.e., 2.94 × 10^{-7} m^2 min^{-1}).

The combined effects of temperature and agitation at the molecular level on the sorbent and in the solution (cavitation effects for ultrasonic treatment, microwave agitation) drastically improve mass transfer properties (uptake kinetics). In the case of UT, the temperature variation is not sufficient for inhibiting sorption and the sorption capacities are enhanced due to better accessibility to reactive groups. For microwave irradiation, the outstanding positive impact on mass transfer is partially compensated by a significant decrease in sorption capacities at equilibrium; probably due to the huge temperature variation (under selected experimental conditions). This effect will be confirmed by the comparison of sorption isotherms at different temperatures under the different

Table 2
Effect of agitation mode on U(VI) uptake kinetics – Parameters for the PFORE, PSORE and RIDE models.

Model	Parameter	Sorbent R-Amine				R-Dithizone			
	Mode	MA	UT1	UT2	μW	MA	UT1	UT2	μW
Exper.	$q_{m,exp.}$ (mmol g^{-1})	1.82	2.11	2.35	0.96	1.53	1.74	2.30	0.80
PFORE	$q_{eq,1}$ (mmol g^{-1})	1.78	1.95	2.22	0.95	1.43	1.65	2.19	0.78
	$k_1 \times 10^2$ (min^{-1})	8.00	42.2	46.9	506	5.60	37.9	51.1	513
	R^2	0.996	0.963	0.974	0.988	0.979	0.986	0.965	0.987
	AIC	−161	−141	−144	−114	−135	−168	−138	−118
PSORE	$q_{eq,2}$ (mmol g^{-1})	1.93	2.14	2.43	1.13	1.59	1.82	2.38	0.93
	$k_2 \times 10^2$ (g $mmol^{-1}$ min^{-1})	6.36	27.4	27.6	528	4.93	28.7	32.1	656
	R^2	0.989	0.994	0.995	0.997	0.999	0.996	0.997	0.998
	AIC	−142	−183	−182	−135	−186	−199	−191	−141
RIDE	$D_e \times 10^9$ (m^2 min^{-1})	1.29	4.28	4.13	131	0.687	4.23	3.74	101
	R^2	0.993	0.987	0.991	0.996	0.996	0.993	0.995	0.997
	AIC	−149	−159	−167	−129	−155	−183	−179	−140

MA: mechanical agitation (210 rpm), UT1: ultrasonic treatment – F: 35 kHz; UT2: ultrasonic treatment – F2: 80 kHz; μW: microwave treatment (F: 2.45 GHz).
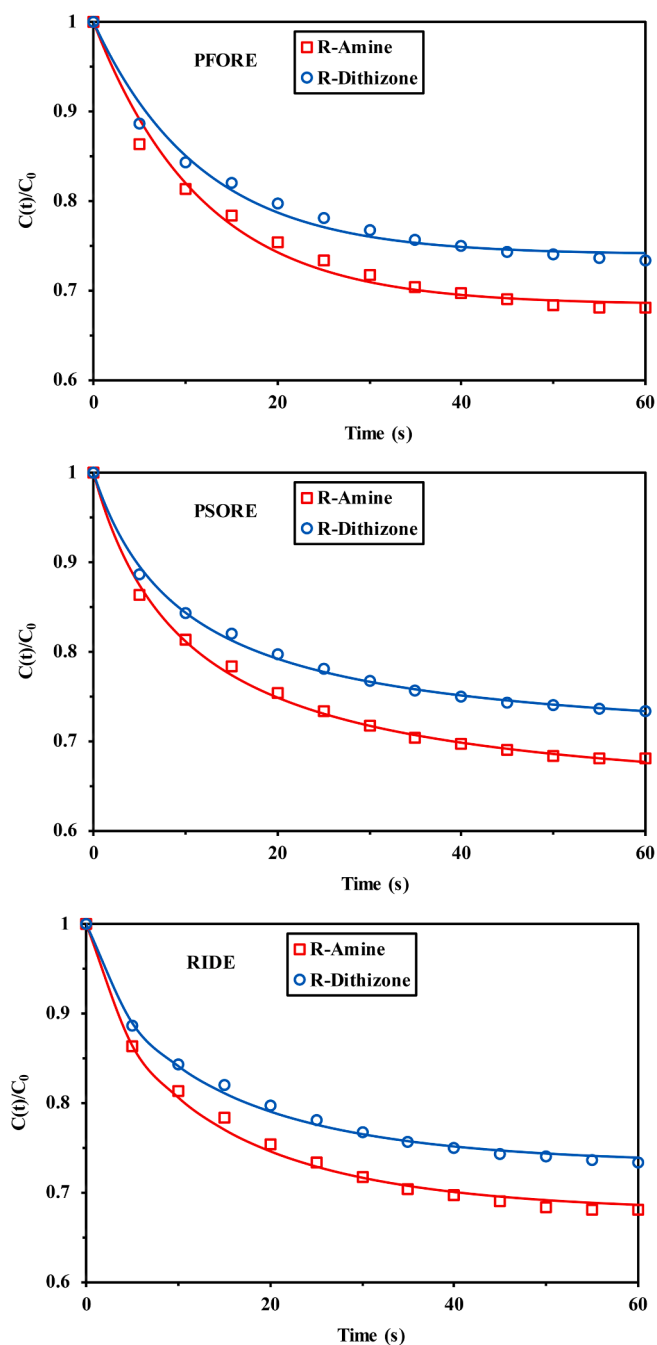
Fig. 3b. Effect of microwave treatment on U(VI) uptake kinetics using R-Amine and R-Dithizone sorbents (Freq.: 2.45 GHz; pH: 5.7; C_0: 3 mM; Sorbent dosage, SD: 1 g L^{-1}; T: 25 ± 1 °C; solid line: PFORE, PSORE, and RIDE modeling).

modes of agitation (following section).

3.2.4. Sorption isotherms

Figure S21 shows the effect of the functionalization of the support (i. e., MCGMA) on U(VI) sorption isotherms. This figure clearly demonstrates the beneficial effect of grafting dithizone and even more DETA on the support. The experimental sorption capacity at saturation is increased 2.6 times and 3.2 times after dithizone- and DETA-functionalization, respectively. The initial slope, which is correlated to the affinity of the sorbent for U(VI) is also strongly increased (4 and 12 times, respectively). These results justify the chemical functionalization of magnetic-GMA-chitosan support (MCGMA).

3.2.4.1. Effect of temperature on sorption isotherms. The thermodynamics of the sorption process was evaluated by comparison of the sorption isotherms for temperatures ranging between 25 °C and 55 °C (Fig. 4). Consistently with the trends observed in section 3.2.3.1., the sorption isotherms are unfavorably influenced by the increase of the temperature. These results confirm the exothermic behavior of U(VI) sorption on R-Amine and R-Dithizone sorbents: both the maximum sorption capacity (sorbent saturation) and the initial slope (correlated to the affinity of the sorbent for target metal) are decreased by increasing the temperature from 25 °C to 55 °C. The Langmuir, Freundlich, and Sips equations have been used for modeling sorption isotherms; Table 3 summarizes the parameters of the models, together with statistic criteria. The asymptotic shape of the isotherms is not consistent with the Freundlich equation (power-like function); this is confirmed by the poor correlation parameters (R^2 and AIC). The introduction of a third-adjustable parameter in the Sips equation (compared with the Langmuir equation) allows slightly increasing the quality of mathematic fits. The values of this third adjustable parameter (i.e., n_S) vary between 0.80 and 1.26; this is close to 1; meaning that the exponent plays a minor role in the global improvement of mathematical fit. In Fig. 4, the solid lines represent the Langmuir fit of experimental profiles (alternative fittings are reported in Figure S22). The Langmuir equation supposes the sorption to occur as a monolayer, without interactions between sorbed molecules, and that the energies involved in the interactions of metal ions with reactive groups are homogeneous (homogeneous reactive groups equally distributed). The calculated sorption capacities ($q_{m,L}$ and $q_{m,S}$) strictly decrease with temperature, consistently with the comparison of experimental values. It is noteworthy that R-Amine systematically exhibits a higher affinity for uranyl ions compared with R-Dithizone; this may be correlated with a higher content of nitrogen-based reactive groups, while S-based reactive groups are softer. Uranyl
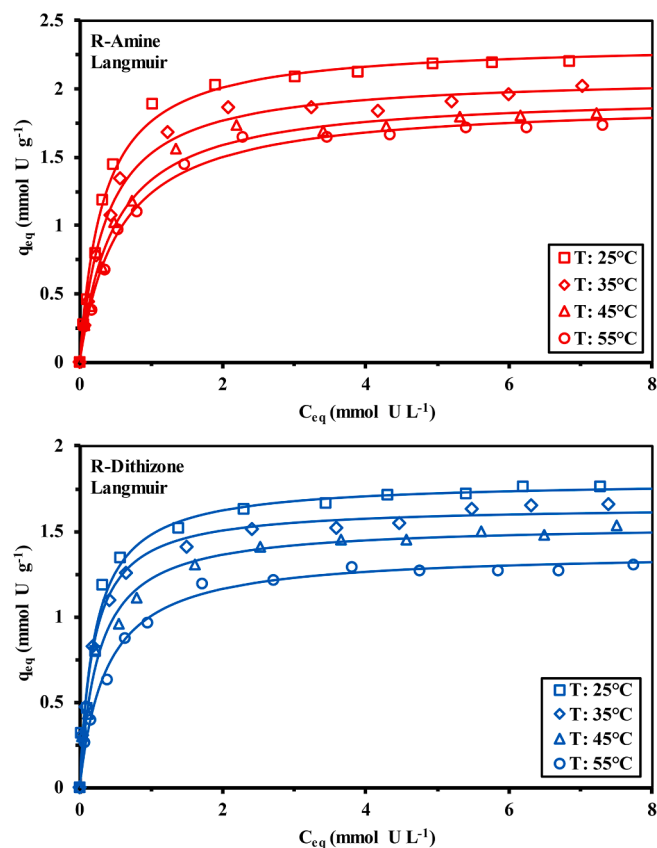

Fig. 4. Effect of temperature on U(VI) sorption isotherms using R-Amine and R-Dithizone sorbents (C_0: 0.33–9 mM; Sorbent dosage, SD: 1 g L^{-1}; T: 25 ± 1 °C; v: 210 rpm; Contact time: 5 h; solid lines: Langmuir modeling).

Table 3

Effect of temperature on U(VI) sorption isotherms under mechanical agitation – Parameters for the Langmuir, Freundlich and Sips equations (additional comparison with U(VI) sorption isotherm onto magnetic-GMA-chitosan support as reference).

Model	Parameter	T °C	Sorbent R-Amine 25	35	45	55	R-Dithizone 25	35	45	55	Magn.-GMA-Chit. 25
Exper.	$q_{m,exp.}$ (mmol g^{-1})		2.20	2.02	1.83	1.74	1.77	1.66	1.52	1.23	0.68
Langmuir	$q_{m,L}$ (mmol g^{-1})		2.34	2.10	1.97	1.91	1.78	1.65	1.57	1.35	0.78
	b_L (L mmol^{-1})		3.05	2.68	2.10	1.84	9.49	5.21	2.73	1.97	0.89
	R^2		0.994	0.994	0.992	0.993	0.962	0.993	0.993	0.993	0.997
	AIC		−68	−71	−69	−73	−50	−74	−74	−77	−109
Freundlich	k_F		1.47	1.29	1.15	1.08	1.35	1.16	0.995	0.78	0.35
	n_F		3.79	3.73	3.54	3.41	5.48	4.74	4.05	3.66	2.84
	R^2		0.911	0.919	0.922	0.928	0.903	0.948	0.953	0.950	0.967
	AIC		−32	−37	−39	−42	−38	−49	−52	−56	−78
Sips	$q_{m,S}$ (mmol g^{-1})		2.24	2.20	1.89	1.83	1.84	1.74	1.68	1.39	0.80
	b_S (L mmol^{-1})		4.57	3.55	2.65	2.25	5.84	3.38	2.00	1.72	0.85
	n_S		0.80	0.844	0.85	0.86	1.23	1.26	1.24	1.11	1.04
	R^2		0.998	0.996	0.994	0.995	0.966	0.996	0.994	0.994	0.997
	AIC		−77	−74	−69	−73	−48	−79	−76	−76	−105

is classified as a hard acid in the HSAB theory (hard and soft acid base concept popularized by Pearson, [104]). Therefore, U(VI) metal ions have a higher affinity for hard bases; logically, the substitution of nitrogen-based groups by sulfur-based groups slightly decreases the affinity of the relevant sorbent for uranyl ions. The affinity coefficients (b_L and b_S) may be used for the application of the van't Hoff equation (Eq. 4) and the determination of thermodynamic parameters [105].

$$Ln\ b_L\ (or\ Ln\ b_S) = -\frac{\Delta H^\circ}{RT} + \frac{\Delta S^\circ}{R} \qquad (4a)$$

$$\Delta G^\circ = \Delta H^\circ - T\Delta S^\circ \qquad (4b)$$

where ΔH° (kJ mol^{-1}), ΔG° (kJ mol^{-1}) and ΔS° (J mol^{-1} K^{-1}) are the changes in enthalpy, Gibbs free energy and entropy, respectively. The values of b_L and b_S are expressed in molar units (L mol^{-1}) according to the discussion of thermodynamic parameters by Lima et al. [105].

Figure S23 shows the relevant plots (for affinity coefficients derived from Langmuir and Sips equations). Table 4 summarizes the thermodynamic parameters for Langmuir affinity coefficients (Table S4, reports the same calculations with the Sips affinity coefficients). The negative values of the enthalpy changes confirm the exothermic behavior of U(VI) sorption on the two sorbents. It is noteworthy that the enthalpy change is much lower for R-Amine than for R-Dithizone (-14.3 kJ mol^{-1} vs. −43.7 kJ mol^{-1}); the variations are less marked considering the calculations issued from Sips equation (Table S4). The differences between R-Amine and R-Dithizone are also strongly marked while considering the entropy change: ΔS° is positive for R-Amine, contrary to R-Dithizone. This means that the sorption of U(VI) on R-Amine is followed by an increase in the disorder of the global system, while the sorption of U(VI) leads to a decrease in the randomness of the system for R-Dithizone. The increased disorder may be associated to H_2O release from hydrated uranyl molecules during sorption on R-Amine. For R-Dithizone the mechanisms may be different due to the presence of alternative reactive groups (S-based sorbent with different binding mechanism), different molecular packing. The free Gibbs energy varies between −19.9 kJ

mol^{-1} and –22.7 kJ mol^{-1} for the different systems and the different temperatures. The reactions are spontaneous; this "spontaneity" is actually poorly influenced by the temperature (based on the weak differences observed). The values of $|\Delta G^\circ|$ are systematically greater than $|T \times \Delta G^\circ|$; this means that the system is controlled by enthalpic changes rather than entropic changes.

3.2.4.2. Effect of agitation mode on sorption isotherms. Uptake kinetics have shown the critical effect of the mode of agitation not only on the mass transfer properties but also on equilibrium performances. This is confirmed by the comparison of sorption isotherms (Fig. 5). The ultrasonic treatment slightly enhances the sorption capacities at saturation; this beneficial effect is hardly increased by using higher frequencies (+10–11%) for R-Amine, while for R-Dithizone the higher frequency (i. e., 80 kHz) allows increasing maximum sorption capacity by 33% (only 15% with F: 35 kHz). On the opposite hand, the microwave irradiation significantly reduces sorption capacities at saturation: by 21% for R-Amine and 52% for R-Dithizone, compared with mechanical agitation. The temperature increase during processing is limited in the case of ultrasonic treatment, at least not enough for making the exothermic behavior of U(VI) sorption significantly depreciating the beneficial effect of cavitation mechanisms (for improving accessibility to reactive groups). It is completely different from microwave irradiation: the increase of temperature up to 90–93 °C reverses a part of metal sorption, which induces a substantial decrease in sorption capacities.

Table 5 confirms these trends when comparing the parameters of the models. The Sips equation fits experimental profiles slightly better than Langmuir equation in most cases. However, the Langmuir equation is more representative of the real mechanisms involved in metal binding; Fig. 5 superposes experimental data and Langmuir fits (Figure S24 shows Sips modeling of experimental curves). The affinity coefficient (correlated with initial slope) is drastically increased by ultrasonic treatment in the case of R-Amine sorbent: by 4.7 times for UT1 agitation, and up to 124 times for UT2 (the enhancement is negligible for

Table 4

Thermodynamic parameters for the sorption of U(VI) using R-Amine and R-Dithizone sorbents (calculations based on b_L parameter).

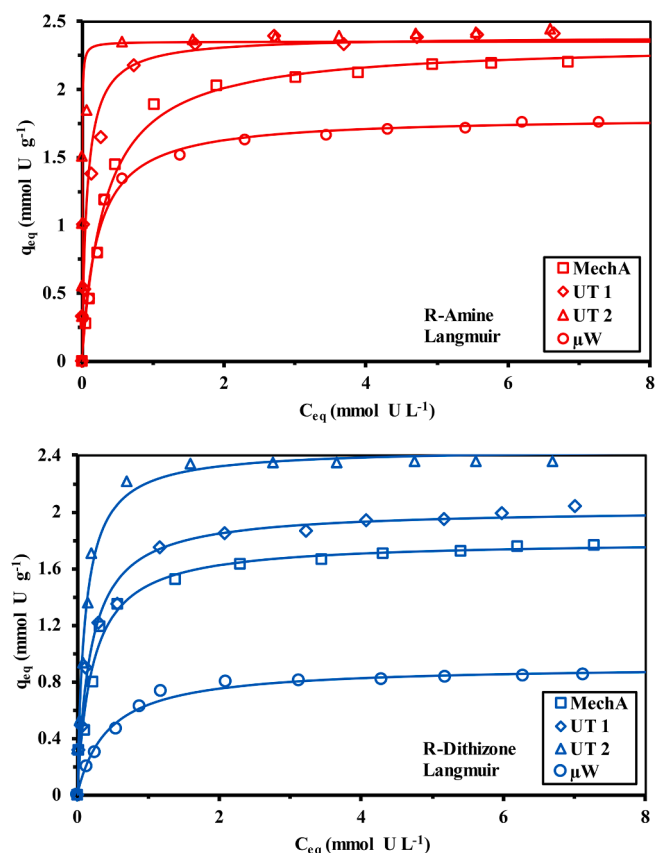| Sorbent	ΔH°(kJ mol^{-1})	ΔS°(J mol^{-1} K^{-1})	R^2	T (°C)	ΔG°(kJ mol^{-1})
R-Amine	−14.34	18.76	0.983	25	−19.93
				35	−20.12
				45	−20.31
				55	−20.49
R-Dithizone	−43.73	−70.8	0.988	25	−22.63
				35	−21.92
				45	−21.21
				55	−20.50

Fig. 5. Effect of agitation mode on U(VI) sorption isotherms using R-Amine and R-Dithizone sorbents (MA: mechanical agitation, UT 1: ultrasonic treatment 37 kHz, UT 2: ultrasonic treatment 80 kHz, μW: microwave treatment 2.45 GHz; C_0: 0.33–9 mM; Sorbent dosage, SD: 1 g L^{-1}; T: 25 ± 1 °C; Contact time: 5 h; solid lines: Langmuir modeling).

microwave irradiation, i.e., 1.5). Surprisingly, in the case of R-Dithizone sorbent, the effect of agitation mode on the affinity coefficient is not clearly established: the affinity coefficient is almost halved under UT1 agitation, it is stabilized with UT2 and strongly reduced with microwave agitation (by a factor 4.2). These differences between R-Amine and R-Dithizone confirm that the binding mechanisms involved in uranyl sequestration are differently affected by the agitation mode and the activation of the reactive groups. It is difficult suggesting a precise interpretation of these contrary effects.

Ultrasonic-assisted sorption (at the highest frequency; i.e., 80 kHz) appears a good compromise in terms of equilibrium performances for promoting U(VI) sorption onto R-Amine both in terms of maximum sorption capacity and affinity. The conclusion is more balanced for R-Dithizone sorbent: the affinity coefficient is comparable for mechanical agitation and UT2 treatment but the ultrasonic treatment at 80 kHz significantly improves maximum sorption capacity. The microwave irradiation, which involves a drastic increase in the temperature (despite short operating time), strongly decreases sorption performances for the two sorbents.

3.2.4.3. Comparison of sorption performances with alternative sorbents. Table 6 summarizes the sorption properties of a series of alternative sorbents whose properties have been recently reported in the literature. The combination of equilibrium and kinetic criteria allows classifying R-Amine as one of the most efficient sorbents for U(VI), especially when the agitation is provided by ultrasonic treatment at the frequency of 80 kHz. Using microwave irradiation allows ultra-fast sorption, at the expense of a decrease in the amount of uranyl that can be bound. Microwave irradiation strongly increases the temperature of the solution, which, in turn, inhibits sorption due to the exothermic behavior of metal binding by reversing the binding mechanism. This property could be used to improve metal desorption from loaded sorbent (see below – Section 3.2.5.1). Functionalized-tubular carbon nanofibers show outstanding sorption properties in terms of both uptake kinetics and maximum sorption capacity. However, the exciting results reported by Ahmad et al. [106] were obtained at pH 8, while most of the leachates are usually produced by acidic treatment (except with carbonate leaching and so on).

3.2.5. Uranium desorption and sorbent recycling
Metal desorption from resins is frequently performed using acidic solutions (including for the release of U(VI) from loaded sorbents). In the case of U(VI), the ability of carbonate to form stable complexes can be also used for developing efficient and selective methods for U(VI) elution. This section examines the effect of agitation mode (standard mechanical agitation *vs.* ultrasonic treatment at frequency F2: 80 kHz and microwave irradiation) for eluents of variable Na_2CO_3 concentration. The presence of 0.1 M H_2O_2, may have a dual effect for increasing the elution efficiency: (a) as an oxidizing agent to maintain uranium under its uranyl form, and (b) the ability to form stable uranyl peroxo-carbonate complex [72].

3.2.5.1. Desorption kinetics – Effects of carbonate concentration and agitation mode. Fig. 6 compares the kinetic profiles (relative release of U (VI) *vs.* sorbed amount, $A(t)/A_0$ for the desorption of U(VI) using MA,

Table 5
Effect of agitation mode on U(VI) sorption isotherms – Parameters for the Langmuir, Freundlich, and Sips equations.

Model			Sorbent R-Amine				R-Dithizone			
	Parameter	Mode	MA	UT1	UT2	μW	MA	UT1	UT2	μW
Exper.	$q_{m,exp.}$ (mmol g^{-1})		2.20	2.41	2.45	1.74	1.77	2.04	2.36	0.853
Langmuir	$q_{m,L}$ (mmol g^{-1})		2.34	2.39	2.35	1.80	1.78	2.02	2.45	0.917
	b_L (L $mmol^{-1}$)		3.05	14.3	377	4.68	9.49	5.28	9.12	2.28
	R^2		0.994	0.949	0.978	0.984	0.962	0.986	0.988	0.990
	AIC		−68	−35	−48	−61	−50	−59	−55	−88
Freundlich	k_F		1.47	1.88	2.11	1.26	1.35	1.42	1.85	0.57
	n_F		3.79	5.59	8.69	4.74	5.48	4.55	5.37	4.25
	R^2		0.911	0.920	0.913	0.933	0.903	0.947	0.903	0.908
	AIC		−32	−31	−30	−43	−38	−43	−29	−59
Sips	$q_{m,S}$ (mmol g^{-1})		2.24	2.67	2.41	1.84	1.84	2.18	2.41	0.877
	b_S (L $mmol^{-1}$)		4.57	3.87	39.9	3.81	5.84	2.94	12.51	3.04
	n_S		0.80	1.71	1.53	1.13	1.23	1.35	0.88	0.80
	R^2		0.998	0.967	0.983	0.984	0.966	0.990	0.990	0.994
	AIC		−77	−39	−48	−58	−48	−61	−52	−91

MA: mechanical agitation (210 rpm), UT1: ultrasonic treatment – F: 35 kHz; UT2: ultrasonic treatment – F2: 80 kHz; μW: microwave treatment (F: 2.45 GHz).

Table 6

Comparison of U(VI) sorption properties of selected sorbents.

Sorbent	pH	Time	$q_{m,L}$	b_L	Ref.
Duolite ES-467	3	90	0.33	10.9	[26]
Functionalized magnetic resin	0.5	180	0.83	5.47	[30]
Functionalized nonwowen fabrics	4	720	0.087	119	[113]
Magnetic *Momordica charantia* leaf	5	120	1.05	8.57	[114]
Montmorillonite colloid	3	30	0.076	187	[115]
201 X 8 ion exchange resin	(a)	180	0.28	5.71	[17]
n-hydroxyapatite-AC/Alginate	5	420	0.078	0.95	[116]
Urea-formaldehyde resin	6	180	0.37	381	[117]
Ca-Rectorite/CMC	5	720	0.102	0.23	[118]
Amine-functionalized magnetic m-SiO$_2$	6	300	1.66	30.1	[31]
Muulti-biopolymer composite	6	1440	0.43	65.0	[119]
Immobilized *Y. lipolyfica* biomass	7.5	60	0.102	2.86	[120]
GO nanoribbons/chitosan composite	5	120	1.40	14.3	[121]
Amidoxime-functionalized marine fungus	6	110	1.56	0.38	[122]
p(aminophosphonic)/pGMA/Magn. n-composite	3–4	90	1.14	16.2	[37]
Monmorillonite/Polyamide 6	4.5	30	0.58	6.19	[123]
Nano-scale zerovalent copper	4	60	0.55	2389	[124]
Amino/Carboxyl porous organic polymer	8	180	0.20	9.04	[125]
DETA-Mesoporous silica	6	360	4.48	3.95	[29]
Amidic-succinic acid/Mesoporous silica	6	360	3.39	4.09	[126]
Functionalized tubular carbon nanofibers	8	10	8.10	303	[106]
Magnetic-GMA-Chitosan	2.7	300	0.78	0.89	*This work*
R-Amine – MA	5.7	300	2.34	3.05	
R-Dithizone – MA	5.7	300	1.78	9.49	
R-Amine – UT2	5.7	45	2.35	377	
R-Dithizone – UT2	5.7	45	2.45	9.12	
R-Amine – µW	5.7	1	1.80	4.68	
R-Dithizone – µW	5.7	1	0.853	2.28	

Time: min; $q_{m,L}$: mmol U L^{-1}; b_L: L mmol^{-1}; (a): acidic sulfuric leachate.

UT2, and µW treatments, and variable concentrations of sodium carbonate. Metal loadings for the different tests are summarized in Table S5 (metal-loaded samples collected from relevant uptake kinetics). The mode of agitation is also a critical parameter for desorption. In the case of mechanical agitation, the efficiency of desorption increases with the concentration of sodium carbonate. However, even at the highest tested concentration (i.e., 0.4 M), the metal is not completely eluted: desorption yield remains below 85%, even after 110 min of contact. Apparently, U(VI) desorption is a little faster for R-Amine sorbent than for R-Dithizone material; however, regardless of sodium carbonate concentration, the equilibrium desorption is comparable for the two sorbents. In the case of UT2, the desorption kinetics are faster: the equilibrium is reached within 10 to 30 min; the equilibrium is reached faster when the concentration of sodium carbonate solution is 0.3 M. In addition, uranyl desorption reaches 97% for both R-Amine and R-Dithizone sorbents while using 0.3 M Na$_2$CO$_3$/0.1 M H$_2$O$_2$ eluent within 30 min of contact. Microwave irradiation allows reaching a desorption yield close to 98% within only one minute of contact: the sorption is completely reversible, providing the concentration of sodium carbonate is adjusted to 0.4 M (without hydrogen peroxide).

The kinetic profiles for U(VI) desorption have been modeled using the PFORE and PSORE adapted to desorption processes [107] (Eq. S1 and S2). Table S6 reports the parameters of the models for the different systems. The PSORE fits systematically better the kinetic profiles than the PFORE for mechanical agitation and ultrasonic treatment, contrary to microwave irradiation experiments that follow the PFORE. As expected, the desorbed amounts (i.e., $q_{d,1}$, equivalent desorption capacity, mmol U g^{-1}) and the apparent rate coefficients of desorption (i.e., k_{d1} or k_{d2}) increase with the concentration of sodium carbonate. The values of desorption capacities are significantly lower than initial U loading in the sorbents, especially for mechanical agitation. For UT2, at the highest sodium carbonate concentrations, the calculated desorption capacities
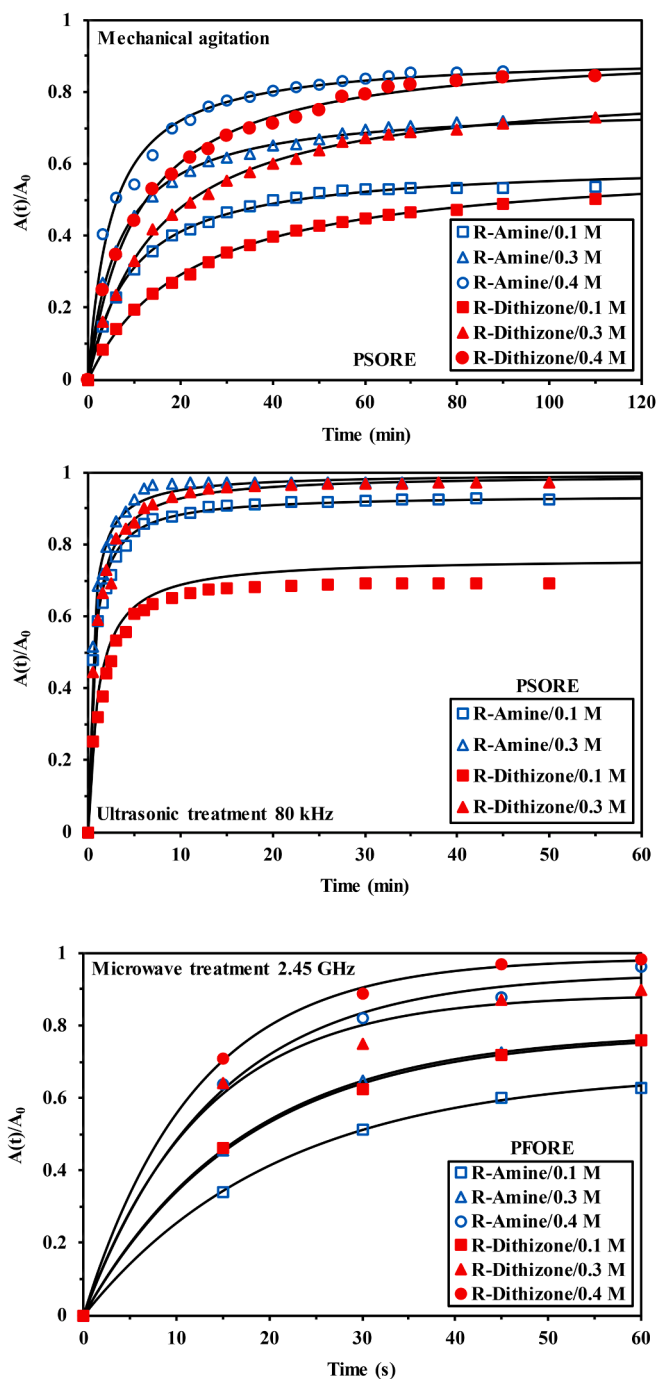

Fig. 6. Effect of Na$_2$CO$_3$ concentration and agitation mode on U(VI) desorption kinetics using R-Amine and R-Dithizone sorbents – Relative desorption ratio (A(t)/A$_0$) and fitting with PSORE or PFORE models (eluent: 0.1 M H$_2$O$_2$ + Na$_2$CO$_3$; SD: 5 g L^{-1}; loaded samples collected from specific uptake kinetics: MA, UT F2, and µW, see above; q_0 (see Table S5).

converge to the initial metal loading for R-Dithizone (while the calculated values overestimate experimental loading with R-Amine sorbent). The apparent rates of desorption are higher for R-Amine than for R-Dithizone. The differences are more marked than for the uptake kinetics (Table 2). The activation energy found for sorption is higher for R-Amine than for R-Dithizone; this is not consistent with the faster desorption of R-Amine. In the case of microwave irradiation, the PFORE allows better fitting experimental profiles than the PSORE. The number of experimental points being limited, the conclusions should be taken as indicative. The yield of desorption increases with sodium carbonate

(comparison of calculated desorption capacities with effective initial metal loading) and the apparent rate coefficients (i.e., k_{d1}) increase with eluent concentration; being slightly superior for R-Dithizone than for R-Amine. In this case, the evolution of rate coefficients is consistent with the respective energies of activation. It is noteworthy that the apparent rate coefficients are of the same order of magnitude for sorption and desorption steps.

The appropriate choice of the agitation mode allows increasing both desorption efficiency and desorption speed but also decreasing the concentration of sodium carbonate to be used. A good compromise would consist in ultrasonic treatment (at frequency: 80 kHz) with a 0.3 M Na_2CO_3 solution (completed with 0.1 M H_2O_2). Complementary tests would be necessary to evaluate the potential of microwave irradiation for effective uranyl desorption, with special attention to the stability of the sorbents.

3.2.5.2. Sorbent recycling. The recycling of the sorbent is also a critical point for the design of the sorption process. In order to evaluate the possibility to re-use the sorbents, a series of five successive cycles of sorption and desorption was performed using UT2 with 0.3 M Na_2CO_3/ 0.1 M H_2O_2. Table 7 summarizes the sorption capacity obtained at each step and the desorption efficiency (individual step and cumulative desorption) for the two sorbents. In the case of R-Amine, the sorption capacity progressively decreases with recycling; however, the loss in sorption performance does not exceed 8% at the fifth cycle. The desorption of U(VI) is highly efficient (between 95.6% and 100%, with cumulative desorption close to 99% at the fifth cycle). In the case of R-Dithizone, the sorption capacity also progressively decreases with sorbent recycling from 2.39 mmol U g^{-1} (saturated sorbent, based on sorption isotherm data for UT2 agitation process) to 2.15 mmol U g^{-1}. At the fifth cycle, the sorption capacity is decreased by 10%. The efficiency of desorption is also highly efficient at each cycle (higher than 98%) and apparently U(VI) is completely desorbed at the fifth cycle.

The recycling induces a weak loss in sorption performance. Since, the desorption yield is remarkably high this loss may be attributed to chemical evolution (or degradation) of the sorbent. In order to verify this hypothesis, the study was completed by the FTIR characterization of the sorbents at the different steps in the five cycles. The spectra did not show significant differences (see Section 3.1.2.): this stability of the materials confirm the good sorption and desorption performances. The sorbents are chemically stable and maintain good performances for at least five cycles.

3.2.5.3. Aging of R-Dithizone sorbent. The sulfur groups at the surface of sorbents are very sensitive to oxidation phenomena; this is usually characterized by a loss in sorption properties with sorbent aging. In order to verify the storage stability of R-Dithizone, a series of experiments performed under similar conditions was performed, in duplicate, with sorbent freshly prepared and stored for 4 and 11 months, without any specific storage conditions (i.e., air atmosphere, dark storage flask).

Figure S25 shows a slight decrease in sorption properties with increasing storage time. After 11 months of storage, the sorbent loses between 17% and 19% in terms of U(VI) sorption capacity. Wu et al. [108] functionalized Amberlite XAD-2 with dithizone for developing a cadmium-sorbent. They observed a good stability of sorption properties on a much shorter storage time (about 1 month). Similar short-term stabilities (about 1 week) were reported for dithizone-bound solid-phase extractant (Zorbax XDB-C18 column) [109].

3.3. Application to uranium recovery from acidic leachates of Red Sea sediments

In order to evaluate the sensitivity of the sorbents to the composition of the solution, a complementary study focused on the treatment of acidic leachates of marine sediments collected on the Jeddah coast (Saudi Arabia). Different acids were used to promote the extraction of many different metals (and arsenic); Table 8 reports the concentrations of 11 elements in the leachate (after pH control to optimized pH value; i. e., pH 5.7). These concentrations are relatively low: the highest concentrations were obtained for iron (i.e., 2.6 mg Fe L^{-1}) and manganese (i. e., 0.24 mg Mn L^{-1}). Uranium concentration does not exceed 3.9 µg L^{-1} (i. e., much lower than the other possible competitor ions, especially base metals). Two series of tests were performed in the presence and the absence of Complexon III (disodium EDTA), which is a well-known ligand efficient for the complexation of metal cations. This masking agent is frequently used for improving the selectivity for the sorption of target metals [110]. Table 8 also reports the distribution coefficients for the different elements and the different systems (sorbent, presence *vs.* absence of Complexon III). This table shows that the two sorbents can bind all the referenced elements with a marked preference for Cu > Zn > Co ~ Cd > Hg ~ Pb ~ Fe ~ Ni > U ~ As > Mn, in the case of R-Amine and

Hg > Cu > Pb > Zn ~ Co > Cd ~ U > As ~ Ni ~ Fe > Mn, in the case of R-Dithizone.

The strong affinity of Hg(II) for sulfur ligands may explain the specific sorption of R-Dithizone. Copper(II) and Pb(II) are the other metal ions that show good binding on R-Dithizone. According to Pearson's rules, U(VI), Fe(III), Mn(II) are classified as hard acids, which may have strong interactions with strong bases (including amine groups). Cadmium(II) and Hg(II) are soft acids, which are supposed to react preferentially with soft bases (including sulfur-based groups). Other divalent cations (i.e., Cu(II), Zn(II), Pb(II), Ni(II), and Co(II)) are members of the so-called borderline class. The ranking appearing above does not follow Pearson's rules and it is difficult predicting distribution coefficients ranking with reference to electronegativity [111] or hydrated radius [112]. The addition of Complexon III into the leachate drastically changes the distribution of metal ions: the strong ability of EDTA to complex divalent cations reduces the availability of the sorbent to bind

Table 7
Sorption and desorption cycles for U recovery using R-Amine and R-Dithizone sorbents (sorption and desorption under ultrasonic treatment at 80 kHz frequency).

Sorbent Cycle	R-Amine			R-Dithizone		
	Adsorption q (mmol g^{-1})	Desorption DE$_{#i}$ (%)	DE$_{cumul.}$ (%)	Adsorption q (mmol g^{-1})	Desorption DE$_{#i}$ (%)	DE$_{cumul.}$ (%)
1	2.51	97.3	97.3	2.39	98.4	98.4
2	2.42	99.7	98.4	2.30	99.4	98.9
3	2.50	95.6	97.5	2.21	100	99.7
4	2.38	100	98.2	2.16	100	100
5	2.31	100	99.2	2.15	100	100

DE$_{#i}$: desorption efficiency at individual step, DE$_{cumul.}$: cumulative desorption efficiency.

Table 8
Comparison of distribution ratios (L kg^{-1}) for selected elements in the treatment of leachates of seawater sediments using R-Amine and R-Dithizone sorbents – Effect of Complexon III (EDTA disodium salt, $C_{10}H_{14}N_2Na_2O_8 \cdot 2H_2O$) on metal selectivity.

Element	C_0 (µg L^{-1})	Without Complexon III		With Complexon III	
		R-Amine	R-Dithizone	R-Amine	R-Dithizone
U	3.9	250.0	439.1	64,000	129,000
Fe	2631.9	316.3	191.1	3.97	1.75
Mn	242.5	105.8	60.34	15.49	6.22
Cu	25.2	6139	3737	140.3	54.39
Zn	43.1	865.8	995.4	0	36.06
Pb	25.4	322.2	1224	7.94	90.13
Ni	40.8	311.9	214.3	17.46	12.41
Cd	6.9	806.3	455.7	11.73	29.85
Co	4.9	808.1	991.9	40.34	20.83
Hg	2.3	337.2	4610	0	45.45
As	12.3	239.9	215.4	8.20	8.20

those metal ions. The poor complexation of uranyl ions by EDTA may explain the higher distribution coefficients found for U(VI): 64 L g^{-1} and 129 L g^{-1} for R-Amine and R-Dithizone, respectively; while the distribution ratios are systematically lower than 0.140 L g^{-1} for the other elements.

The beneficial effect of Complexon III on sorption efficiency is also demonstrated in Table S7. In absence of Complexon III, the two sorbents have a large reactivity for selected elements; with sorption efficiencies ranging between 6% (for manganese) and up to 86% (for copper). On the opposite hand, the efficiency of U(VI) sorption reaches 99%; the complexation of metal cations by EDTA allows more reactive groups to be free and available for uranium. The complexation of metal ions limits their sorption onto R-Amine (less than 4%), except for copper (up to 12%). For R-Dithizone, the presence of sulfur-groups maintains sorption for Pb(II) (8%), Cu(II) (5%), Hg(II) (4%), Zn(II) (3.5%) and Cd(II) (3%). These sulfur-groups decrease the selectivity of the sorbent for U(VI).

Table S8 reports the distribution ratio D_C/D_0 of each individual metal, as the ratio of distribution ratio in the presence of Complexon III (D_c) to the D_0 value in absence of ligand. This ratio allows illustrating the singular effect of Complexon III on the removal of uranium against other elements: D_C/D_0 varies in the range 256–294 for U(VI) while for other metals (and As) the ratio never exceeds 0.15. In order to highlight this selectivity effect, the selectivity coefficient for U over other elements is calculated as $SC_{U/Me} = D_U/D_{Me}$. This selectivity coefficient was compared in the absence ($SC^0_{U/Me}$) and presence of Complexon III ($SC^C_{U/Me}$). The corresponding ratio ($SC^C_{U/Me}/SC^0_{U/Me}$) can be used for highlighting the positive impact of the complexing agent on the selectivity of the sorbents for U(VI). For R-amine, the highest selectivity enhancements are obtained for Zn (virtually ∞), Hg (virtually ∞), Fe (20413), and Cd (17596):

Zn ~ Hg≫Fe > Cd≫Cu ~ Pb > As > Co > Ni > Mn.

For R-Dithizone, the enhancement effect is ranked according to the series:

Fe ~ Hg≫Cu≫Co≫Zn > As > Ni > Cd > Pb > Mn.

The addition of Complexon III in the leachate allows increasing the efficiency and the selectivity of the sorbent for U(VI) as a good tool for concentrating and separating this metal from the other metal ions. This may be useful for the analytical purpose for limiting the competitive effect of other metal cations, for improving the efficiency of metal recovery, and for reducing the interfering effect in the other steps of metal analysis.

4. Conclusion

A simple method has been designed for preparing two functionalized magnetic chitosan nanoparticles, through the grafting of glycidyl methacrylate, followed by insertion of either amine groups (using DETA) or dithizone.

The main achievements of this work consist of:

(a) the extensive evaluation of the beneficial effect of high frequency (i.e., 80 kHz) ultrasonic treatment on the improvement of accessibility of internal reactive groups to sorbate molecules (associated with enhanced mass transfer properties).

(b) the evaluation of thermodynamics for sorption processes, which correlate well with observed sorption properties: exothermic sorption may explain the negative effect of microwave irradiation on sorption performance (due to strong temperature increase) but the very beneficial impact on desorption (reducing required time for complete desorption with lower eluent concentration).

(c) the design of an optimized process combining ultrasonic-boosted sorption and microwave-activated desorption.

(d) the remarkable stability of R-Amine sorbent allowing its successful recycling.

(e) the global superiority of R-Amine compared with R-Dithizone for uranyl sorption.

(f) the extensive characterization of sorbent (using many different analytical facilities).

(g) the efficiency of the sorbent for separation of U(VI) from other metal ions from complex solutions, especially in the presence of Complexon III.

The combination of these different characteristics, extensive investigation, and specific properties (highlighted by high sorption capacities, fast kinetics, and recyclability) demonstrates the remarkable potential of R-Amine under optimized conditions (sorption/desorption).

The most emblematic results for optimized sorption and desorption correspond to a maximum sorption capacity close to 2.2 mmol U g^{-1} using R-Amine, at pH$_0$ ~ 5. The equilibrium is reached within 30 min of contact under ultrasonic treatment (at 80 kHz frequency). The desorption of uranyl from loaded sorbent is achieved using 0.3 M Na$_2$CO$_3$/0.1 M H$_2$O$_2$ solutions under microwave exposure: the increase in the temperature and the fast accessibility to internal reactive groups allows decreasing the concentration of the eluent and reaching the complete desorption within 1 min of contact. While using the ultrasonic treatment for desorption in recycling tests, the sorption and desorption performances are maintained at good levels for a minimum of five cycles. The sorbents have been also successfully tested for the recovery of U(VI) from acidic leachates of sea sediments: the addition of Complexon III (as a masking agent) allows improving the separation of uranium from other metal cations in complex solutions.

This exhaustive study is completed but the extensive characterization of the materials both in terms of physical and chemical properties; not only in terms of structure but also through the interpretation of binding mechanisms. This makes this work remarkably complete and confirms the promising perspectives opened by these materials for uranium recovery from slightly acidic complex solutions.

Declaration of Competing Interest

The authors declare that they have no known competing financial interests or personal relationships that could have appeared to influence the work reported in this paper.

Acknowledgements

Appendix A. Supplementary data

Supplementary data to this article can be found online at https://doi.org/10.1016/j.cej.2021.128553.

References

[1] WHO, Guidelines for Drinking-water Quality, in, WHO, Geneva, Switzerland, 2017.

[2] A.L. Smirnov, V.N. Rychkov, S.M. Titova, N.A. Poponin, K.A. Nalivayko, Precipitation of uranium from nitrate-sulfuric eluates by aqueous ammonia solution, J. Radioanal. Nucl. Chem. 317 (2018) 863–869.

[3] P. Li, P. Chen, G.H. Wang, L.Z. Wang, X.G. Wang, Y.R. Li, W.M. Zhang, H. Jiang, H. Chen, Uranium elimination and recovery from wastewater with ligand chelation-enhanced electrocoagulation, Chem. Eng. J. 393 (2020). Art. N° 124819.

[4] K. Yuan, D. Renock, R.C. Ewing, U. Becker, Uranium reduction on magnetite: Probing for pentavalent uranium using electrochemical methods, Geochim. Cosmochim. Acta 156 (2015) 194–206.

[5] P.L. Liang, L.Y. Yuan, H. Deng, X.C. Wang, L. Wang, Z.J. Li, S.Z. Luo, W.Q. Shi, Photocatalytic reduction of uranium(VI) by magnetic ZnFe$_2$O$_4$ under visible light, Appl. Catal., B, 267 (2020). Art. N° 118688.

[6] E.C. Avelar, C.L.G. Alvarenga, G.P.S. Resende, C.A. Morais, M.B. Mansur, Modeling of the solvent extraction equilibrium of uranium(VI) sulfate with Alamine 336, Braz. J. Chem. Eng. 34 (2017) 355–362.

[7] S. Wu, L. Wang, P. Zhang, H. El-Shall, B. Moudgil, X. Huang, L. Zhao, L. Zhang, Z. Feng, Simultaneous recovery of rare earths and uranium from wet process phosphoric acid using solvent extraction with D2EHPA, Hydrometallurgy 175 (2018) 109–116.

[8] M.A. Mosleh, E.H. El-Hakim, A.Z. Ahmed, M.S. Abd El-Ghany, A.M. El-Didamony, Equilibrium and kinetic studies on uranium sorption from aqueous sulphate medium using tri-n-octylamine impregnated resin, Int. J. Environ. Anal. Chem. (2020). Art. N° 1766038.

[9] A. Gladysz-Plaska, E. Grabias, M. Majdan, Simultaneous adsorption of uranium (VI) and phosphate on red clay, Prog. Nucl. Energy 104 (2018) 150–159.

[10] R. Liao, Z. Shi, Y. Hou, K. Zhang, J. Zhang, X. Wang, K. Cheng, L. Yang, Uranium sorption onto mullite: Characteristics of isotherms, kinetics and thermodynamics, J. Earth Syst. Sci. 128 (2019). Art. N° 176.

[11] R.A. Abou-Lilah, H.E. Rizk, M.A. Elshorbagy, A.M. Gamal, A.M. Ali, N.A. Badawy, Efficiency of bentonite in removing cesium, strontium, cobalt and uranium ions from aqueous solution: encapsulation with alginate for column application, Int. J. Environ. Anal. Chem. (2020). Art. N° 1761348.

[12] P. Michard, E. Guibal, T. Vincent, P. LeCloirec, Sorption and desorption of uranyl ions by silica gel: pH, particle size and porosity effects, Microporous Mater. 5 (1996) 309–324.

[13] X. Wang, L. Yuan, Y. Wang, Z. Li, J. Lan, Y. Liu, Y. Feng, Y. Zhao, Z. Chai, W. Shi, Mesoporous silica SBA-15 functionalized with phosphonate and amino groups for uranium uptake, Sci. China Mater. 55 (2012) 1705–1711.

[14] D. Humelnicu, M.V. Dinu, E.S. Dragan, Adsorption characteristics of UO_2^{2+} and Th^{4+} ions from simulated radioactive solutions onto chitosan/clinoptilolite sorbents, J. Hazard. Mater. 185 (2011) 447–455.

[15] C. Falaise, C. Volkringer, R. Giovine, B. Prelot, M. Huve, T. Loiseau, Capture of actinides (Th^{4+}, $[UO_2]^{2+}$) and surrogating lanthanide (Nd^{3+}) in porous metal-organic framework MIL-100(Al) from water: selectivity and imaging of embedded nanoparticles, Dalton Trans. 46 (2017) 12010–12014.

[16] H.Y. Wu, F.T. Chi, S. Zhang, J. Wen, J. Xiong, S. Hu, Control of pore chemistry in metal-organic frameworks for selective uranium extraction from seawater, Microporous Mesoporous Mater. 288 (2019). Art. N° 109567.

[17] Z. Wen, K. Huang, Y. Niu, Y. Yao, S. Wang, Z. Cao, H. Zhong, Kinetic study of ultrasonic-assisted uranium adsorption by anion exchange resin, Colloids Surf. A (2020) 585. Art. N° 124021.

[18] R. Karan, K.C. Rajan, T. Sreenivas, Studies on lowering of uranium from mine water by static bed ion exchange process, Sep. Sci. Technol. 54 (2019) 1607–1619.

[19] J.T.M. Amphlett, C.A. Sharrad, R.I. Foster, M.D. Ogden, Ethylenediamine-funtionalized ion exchange resin for uranium recovery from acidic mixed sulphate-chloride media: initial column loading studies, J. South Afr. Inst. Min. Metall. 118 (2018) 1251–1257.

[20] J.T.M. Amphlett, M.D. Ogden, R.I. Foster, N. Syna, K.H. Soldenhoff, C.A. Sharrad, The effect of contaminants on the application of polyamine functionalised ion exchange resins for uranium extraction from sulfate based mining process waters, Chem. Eng. J. 354 (2018) 633–640.

[21] K.L. Ang, D. Li, A.N. Nikoloski, The effectiveness of ion exchange resins in separating uranium and thorium from rare earth elements in acidic aqueous sulfate media. Part 1. Anionic and cationic resins, Hydrometallurgy 174 (2017) 147–155.

[22] M. Solgy, M. Taghizadeh, D. Ghoddocynejad, Adsorption of uranium(VI) from sulphate solutions using Amberlite IRA-402 resin: Equilibrium, kinetics and thermodynamics study, Ann. Nucl. Energy 75 (2015) 132–138.

[23] R.I. Foster, J.T.M. Amphlett, K.-W. Kim, T. Kerry, K. Lee, C.A. Sharrad, SOHIO process legacy waste treatment: Uranium recovery using ion exchange, J. Ind. Eng. Chem. 81 (2020) 144–152.

[24] D.H. Phillips, B. Gu, D.B. Watson, C.S. Parmele, Uranium removal from contaminated groundwater by synthetic resins, Water Res. 42 (2008) 260–268.

[25] N. Kabay, M. Demircioglu, S. Yayli, E. Gunay, M. Yuksel, M. Saglam, M. Streat, Recovery of uranium from phosphoric acid solutions using chelating ion-exchange resins, Ind. Eng. Chem. Res. 37 (1998) 1983–1990.

[26] I.H. Zidan, M.F. Cheira, A.R. Bakry, B.M. Atia, Potentiality of uranium recovery from G.Gattar leach liquor using Duolite ES-467 chelating resin: Kinetic, thermodynamic and isotherm features, Int. J. Environ. Anal. Chem. (2020). Art. N° 1748613.

[27] Z. Liu, D. Liu, Z. Cai, Y. Wang, L. Zhou, Synthesis of new type dipropyl imide chelating resin and its potential for uranium(VI) adsorption, J. Radioanal. Nucl. Chem. 318 (2018) 1219–1227.

[28] K.L. Ang, D. Li, A.N. Nikoloski, The effectiveness of ion exchange resins in separating uranium and thorium from rare earth elements in acidic aqueous sulfate media. Part 2. Chelating resins, Miner. Eng. 123 (2018) 8–15.

[29] P. Amesh, K.A. Venkatesan, A.S. Suneesh, N. Samanta, Diethylenetriamine tethered mesoporous silica for the sequestration of uranium from aqueous solution and seawater, J. Environ. Chem. Eng. 8 (2020). Art. N° 103995.

[30] S. Zhang, D. Yuan, Q. Zhang, Y. Wang, Y. Liu, J. Zhao, B. Chen, Highly efficient removal of uranium from highly acidic media achieved using a phosphine oxide and amino functionalized superparamagnetic composite polymer adsorbent, J. Mater. Chem. A 8 (2020) 10925–10934.

[31] S. Liu, J. Luo, J. Ma, J. Li, S. Li, L. Meng, S. Liu, Removal of uranium from aqueous solutions using amine-functionalized magnetic platelet large-pore SBA-15, J. Nucl. Sci. Technol. (2020). Art. N° 1796838.

[32] C.E. Duval, W.A. Hardy, S. Pellizzeri, T.A. DeVol, S.M. Husson, Phosphonic acid and alkyl phosphate-derivatized resins for the simultaneous concentration and detection of uranium in environmental waters, React. Funct. Polym. 137 (2019) 133–139.

[33] H. Sarafraz, A. Minuchehr, G. Alahyarizadeh, Z. Rahimi, Synthesis of enhanced phosphonic functional groups mesoporous silica for uranium selective adsorption from aqueous solutions, Sci. Rep. 7 (2017). Art. N° 11675.

[34] S.D. Alexandratos, X.P. Zhu, M. Florent, R. Sellin, Polymer-supported bifunctional amidoximes for the sorption of uranium from seawater, Ind. Eng. Chem. Res. 55 (2016) 4208–4216.

[35] X. Lu, D. Zhang, A. Tesfay Reda, C. Liu, Z. Yang, S. Guo, S. Xiao, Y. Ouyang, Synthesis of amidoxime-grafted activated carbon fibers for efficient recovery of uranium(VI) from aqueous solution, Ind. Eng. Chem. Res. 56 (2017) 11936–11947.

[36] M. Ahmad, J. Wang, Z. Yang, Q. Zhang, B. Zhang, Ultrasonic-assisted preparation of amidoxime functionalized silica framework via oil-water emulsion method for selective uranium adsorption, Chem. Eng. J. 389 (2020). Art. N° 124441.

[37] A.A. Galhoum, W.H. Eisa, I.E.-T. El-Sayed, A.A. Tolba, Z.M. Shalaby, S. I. Mohamady, S.S. Muhammad, S.S. Hussien, T. Akashi, E. Guibal, A new route for manufacturing poly(aminophosphonic)-functionalized poly(glycidyl methacrylate)-magnetic nanocomposite - Application to uranium sorption from ore leachate, Environ. Pollut 264 (2020). Art. N° 114797.

[38] K.Z. Elwakeel, A.A. Atia, E. Guibal, Fast removal of uranium from aqueous solutions using tetraethylenepentamine modified magnetic chitosan resin, Bioresour. Technol. 160 (2014) 107–114.

[39] A.R. Elsalamouny, O.A. Desouky, S.A. Mohamed, A.A. Galhoum, E. Guibal, Uranium and neodymium biosorption using novel chelating polysaccharide, Int. J. Biol. Macromol. 104 (2017) 963–968.

[40] M.F. Hamza, J.-C. Roux, E. Guibal, Uranium and europium sorption on amidoxime-functionalized magnetic chitosan micro-particles, Chem. Eng. J. 344 (2018) 124–137.

[41] M.G. Mahfouz, A.A. Galhoum, N.A. Gomaa, S.S. Abdel-Rehem, A.A. Atia, T. Vincent, E. Guibal, Uranium extraction using magnetic nano-based particles of diethylenetriamine-functionalized chitosan: Equilibrium and kinetic studies, Chem. Eng. J. 262 (2015) 198–209.

[42] L.C.B. Stopa, M. Yamaura, Uranium removal by chitosan impregnated with magnetite nanoparticles: adsorption and desorption, Int. J. Nucl. Energy Sci. Technol. 5 (2010) 283–289.

[43] M. Behbahani, M. Najafi, M.M. Amini, O. Sadeghi, A. Bagheri, M. Salarian, Dithizone-modified nanoporous fructose as a novel sorbent for solid-phase extraction of ultra-trace levels of heavy metals, Microchim. Acta 180 (2013) 911–920.

[44] M. Behbahani, M. Salarian, M.M. Amini, O. Sadeghi, A. Bagheri, S. Bagheri, Application of a new functionalized nanoporous silica for simultaneous trace separation and determination of Cd(II), Cu(II), Ni(II), and Pb(II) in food and agricultural products, Food Anal. Methods 6 (2013) 1320–1329.

[45] H.M. Marwani, H.M. Albishri, T.A. Jalal, E.M. Soliman, Activated carbon immobilized dithizone phase for selective adsorption and determination of gold (III), Desalin. Water Treat. 45 (2012) 128–135.

[46] H. Hashemi-Moghaddam, F. Yahyazadeh, M.T. Vardini, Synthesis of a new molecularly imprinted polymer for sorption of the silver ions from geological and antiseptic samples for determination by flame atomic absorption spectrometry, J. AOAC Int. 97 (2014) 1434–1438.

[47] L. Zhang, Z. Xiong, L. Zhang, B. Yu, W. Zhang, Magnetic nanoparticles coated with dithizone-modified chitosan for use in solid-phase extraction of copper(II), Anal. Methods 7 (2015) 2050–2054.

[48] J. Fu, X. Wang, J. Li, Y. Ding, L. Chen, Synthesis of multi-ion imprinted polymers based on dithizone chelation for simultaneous removal of Hg^{2+}, Cd^{2+}, Ni^{2+} and Cu^{2+} from aqueous solutions, RSC Adv. 6 (2016) 44087–44095.

[49] S.S. Lins, C.F. Virgens, W.N. Lopes dos Santos, I.H. Santos Estevam, G.C. Brandao, C.S. Assis Felix, S.L. Costa Ferreira, On-line solid phase extraction system using an ion imprinted polymer based on dithizone chelating for selective preconcentration and determination of mercury(II) in natural waters by CV AFS, Microchem. J. 150 (2019). Art. N° 104075.

[50] H. Abdolmohammad-Zadeh, R. Mohammad-Rezaei, A. Salimi, Preconcentration of mercury(II) using a magnetite@carbon/dithizone nanocomposite, and its quantification by anodic stripping voltammetry, Microchim. Acta 187 (2020). Art. N° 2.

[51] A.R.L. Spies, F. Wewers, Equilibrium, kinetics and thermodynamics studies of Cd sorption onto a dithizone-impregnated Amberchrom CG-300m polymer resin, Arabian J. Chem. 13 (2020) 5050–5059.

[52] S.R. Gadjieva, F.N. Bahmanova, E.N. Alirzaeva, N.T. Shamilov, F.M. Chyragov, Sorption concentration of uranium in sea water using a polymer sorbent containing fragments of dithizone, J. Water Chem. Technol. 41 (2019) 94–100.

[53] K.Z. Elwakeel, A. Shahat, Z.A. Khan, W. Alshitari, E. Guibal, Magnetic metal oxide-organic framework material for ultrasonic-assisted sorption of titan yellow and rose bengal from aqueous solutions, Chem. Eng. J. 392 (2020). Art. N° 123635.

[54] K.Z. Elwakeel, A. Shahat, A.S. Al-Bogami, B. Wijesiri, A. Goonetilleke, The synergistic effect of ultrasound power and magnetite incorporation on the sorption/desorption behavior of Cr(VI) and As(V) oxoanions in an aqueous system, J. Colloid Interface Sci. 569 (2020) 76–88.

[55] A. Mary Elias, M.P. Saravanakumar, A critical review on ultrasonic-assisted dye adsorption: Mass transfer, half-life and half-capacity concentration approach with future industrial perspectives, Crit. Rev. Env. Sci. Technol. 49 (2019) 1959–2015.

[56] M. Behbahani, V. Zarezade, A. Veisi, F. Omidi, S. Bagheri, Modification of magnetized MCM-41 by pyridine groups for ultrasonic-assisted dispersive micro-solid-phase extraction of nickel ions, Int. J. Environ. Sci. Technol. 16 (2019) 6431–6440.

[57] W.-B. Zhang, M. Deng, C.-X. Sun, S.-B. Wang, Ultrasound-enhanced adsorption of chromium(VI) on Fe_3O_4 magnetic particles, Ind. Eng. Chem. Res. 53 (2014) 333–339.

[58] M. Sheydaei, A.B. Gasemsoltanlu, A. Beiraghi, Optimization of ultrasonic-assisted copper ion removal from polluted water by a natural clinoptilolite nanostructure through a central composite design, Clay Minerals 54 (2019) 339–347.

[59] M. Behbahani, F. Omidi, M.G. Kakavandi, G. Hesam, Selective and sensitive determination of silver ions at trace levels based on ultrasonic-assisted dispersive solid-phase extraction using ion-imprinted polymer nanoparticles, Appl. Organomet. Chem. 31 (2017), e3758.

[60] M. Behbahani, S. Bagheri, F. Omidi, M.M. Amini, An amino-functionalized mesoporous silica (KIT-6) as a sorbent for dispersive and ultrasonication-assisted micro solid phase extraction of hippuric acid and methylhippuric acid, two biomarkers for toluene and xylene exposure, Microchim. Acta 185 (2018) 505.

[61] M. Behbahani, A. Veisi, F. Omidi, A. Noghrehabadi, A. Esrafili, H.R. Sobhi, The conjunction of a new ultrasonic-assisted dispersive solid-phase extraction method with HPLC-DAD for the trace determination of diazinon in biological and water media, New J. Chem. 42 (2018) 4289–4296.

[62] S. Deng, G. Zhang, Y. Li, Y. Dou, P. Wang, Facile preparation of amidoxime-functionalized fiber by microwave-assisted method for the enhanced adsorption of chromium(VI) from aqueous solution, RSC Adv. 6 (2016) 64665–64675.

[63] J. Spooren, T.A. Atia, Combined microwave assisted roasting and leaching to recover platinum group metals from spent automotive catalysts, Miner. Eng. 146 (2020). Art. N° 106153.

[64] K.Z. Elwakeel, A.M. Elgarahy, G.A. Elshoubaky, S.H. Mohammad, Microwave assist sorption of crystal violet and Congo red dyes onto amphoteric sorbent based on upcycled Sepia shells, J. Environ. Heath Sci. 18 (2020) 35–50.

[65] A.M. Elgarahy, K.Z. Elwakeel, G.A. Elshoubaky, S.H. Mohammad, Microwave-accelerated sorption of cationic dyes onto green marine algal biomass, Environ. Sci. Pollut. Res. 26 (2019) 22704–22722.

[66] M.E. Mahmoud, M.M. Osman, H. Abdel-Aal, G.M. Nabil, Microwave-assisted adsorption of Cr(VI), Cd(II) and Pb(II) in presence of magnetic graphene oxide-covalently functionalized-tryptophan nanocomposite, J. Alloys Compd. 823 (2020). Art. N° 153855.

[67] M.E. Mahmoud, S.S.M. Hassan, A.H. Kamel, M.I.A. Elserw, Efficient and fast microwave sorption of heavy metals on nanosilica sorbents-microwave immobilized-vitamin C and vitamin L1, J. Environ. Chem. Eng. 7 (2019). Art. N° 102850.

[68] K.Z. Elwakeel, A.S. Al-Bogami, E. Guibal, 2-Mercaptobenzimidazole derivative of chitosan for silver sorption – Contribution of magnetite incorporation and sonication effects on enhanced metal recovery, Chem. Eng. J. 403 (2021). Art. N° 126265.

[69] R. Massart, Preparation of aqueous magnetic liquids in alkaline and acidic media, IEEE Trans. Magn. 17 (1981) 1247–1249.

[70] S.B. Savvin, Analytical use of arsenazo III: Determination of thorium, zirconium, uranium and rare earth elements, Talanta 8 (1961) 673–685.

[71] A.K. Nayak, A. Pal, Development and validation of an adsorption kinetic model at solid-liquid interface using normalized Gudermannian function, J. Mol. Liq. 276 (2019) 67–77.

[72] H.B. Pan, W.S. Liao, C.M. Wai, Y. Oyola, C.J. Janke, G.X. Tian, L.F. Rao, Carbonate-H_2O_2 leaching for sequestering uranium from seawater, Dalton Trans. 43 (2014) 10713–10718.

[73] R. Baghaliannejad, M. Aghahoseini, M.K. Amini, Determination of rare earth elements in uranium materials by ICP-MS and ICP-OES after matrix separation by solvent extraction with TEHP, Talanta, 222 (2021) Art. N° 121509.

[74] Y. Wang, X. Hou, W. Zhang, L. Zhang, Y. Fan, Determination of ultra-low 236U in environment samples using ICP-MS/MS measurement and chemical separation, Talanta, 224 (2021) Art. N° 121882.

[75] M.A. Rosanoff, A.E. Hill, A necessary modification of Volhard's method for the determination of chlorides, JACS 29 (1907) 269–275.

[76] T.N. Kropacheva, A.S. Antonova, Y.V. Rabinovich, V.I. Kornev, Complexons as reagents for demetallization of contaminated sediments, Russ. J. Appl. Chem. 87 (2014) 1422–1429.

[77] G.A. Kloster, M. Valiente, N.E. Marcovich, M.A. Mosiewicki, Adsorption of arsenic onto films based on chitosan and chitosan/nano-iron oxide, Int. J. Biol. Macromol. 165 (2020) 1286–1295.

[78] L. Lv, N. Chen, C. Feng, J. Zhang, M. Li, Heavy metal ions removal from aqueous solution by xanthate-modified cross-linked magnetic chitosan/poly(vinyl alcohol) particles, RSC Adv. 7 (2017) 27992–28000.

[79] H. Zhang, Q. Dang, C. Liu, D. Yu, Y. Wang, X. Pu, Y. Liu, Y. Liang, D. Cha, Fabrication of methyl acrylate and tetraethylenepentamine grafted magnetic chitosan microparticles for capture of Cd(II) from aqueous solutions, J. Hazard. Mater. 366 (2019) 346–357.

[80] T.M. Freire, L.M.U.D. Fechine, D.C. Queiroz, R.M. Freire, J.C. Denardin, N.M.P.S. Ricardo, T.N.B. Rodrigues, D.R. Gondim, I.J.S. Junior, P.B.A. Fechine, Magnetic porous controlled Fe3O4-chitosan nanostructure: An ecofriendly adsorbent for efficient removal of azo dyes, Nanomaterials, 10 (2020) Art. N° 10061194.

[81] N. Habibi, Preparation of biocompatible magnetite-carboxymethyl cellulose nanocomposite: Characterization of nanocomposite by FTIR, XRD, FESEM and TEM, Spectrochim. Acta, Part A 131 (2014) 55–58.

[82] N. Salem, A. Ahmad, A. Awwad, New route for synthesis magnetite nanoparticles from ferrous ions and Pistachio leaf extract, J. Nanosci. Nanotechnol. 3 (2013) 48–51.

[83] S. Liang, Z. Ziyu, J. Han, D. Xiaoyan, Facile synthesis of magnetic mesoporous silica spheres for efficient removal of methylene blue via catalytic persulfate activation, Sep. Purif. Technol. 256 (2021), 117801.

[84] G. Dodi, D. Hritcu, G. Lisa, M.I. Popa, Core-shell magnetic chitosan particles functionalized by grafting: Synthesis and characterization, Chem. Eng. J. 203 (2012) 130–141.

[85] A. Khan, S. Badshah, C. Airoldi, Biosorption of some toxic metal ions by chitosan modified with glycidylmethacrylate and diethylenetriamine, Chem. Eng. J. 171 (2011) 159–166.

[86] Z. Cherifi, B. Boukoussa, A. Zaoui, M. Belbachir, R. Meghabar, Structural, morphological and thermal properties of nanocomposites poly (GMA)/clay prepared by ultrasound and in-situ polymerization, Ultrason. Sonochem. 48 (2018) 188–198.

[87] T.A. Arica, E. Ayas, M.Y. Arica, Magnetic MCM-41 silica particles grafted with poly(glycidylmethacrylate) brush: Modification and application for removal of direct dyes, Microporous Mesoporous Mater. 243 (2017) 164–175.

[88] K. Wang, G.M. Qiu, H.Y. Cao, R.F. Jin, Removal of chromium(VI) from aqueous solutions using Fe_3O_4 magnetic polymer microspheres functionalized with amino groups, Materials 8 (2015) 8378–8391.

[89] A. Khan, S. Badshah, C. Airoldi, Environmentally benign modified biodegradable chitosan for cation removal, Polym. Bull. 72 (2015) 353–370.

[90] Z.-Q. Bai, L.-Y. Yuan, L. Zhu, Z.-R. Liu, S.-Q. Chu, L.-R. Zheng, J. Zhang, Z.-F. Chai, W.-Q. Shi, Introduction of amino groups into acid-resistant MOFs for enhanced U(VI) sorption, J. Mater. Chem. A 3 (2015) 525–534.

[91] V. Hiranmayee, K. Ananthasivan, D. Maji, K. Joseph, Microwave-assisted citrate gel-combustion synthesis of nanocrystalline urania, J. Nucl. Mater. 516 (2019) 73–83.

[92] T.J.M. Fraga, L.E.M. de Lima, Z.S.B. de Souza, M.N. CarvalhoE.M.P.d.L. Freire, M.G. Ghislandi, M.A. da Motta,, Amino-Fe_3O_4-functionalized graphene oxide as a novel adsorbent of Methylene Blue: kinetics, equilibrium, and recyclability aspects, Environ. Sci. Pollut. Res. Int 26 (2018) 28593–28602.

[93] Z. Adibmehr, H. Faghihian, Preparation of highly selective magnetic cobalt ion-imprinted polymer based on functionalized SBA-15 for removal Co^{2+} from aqueous solutions, J. Environ. Heath Sci. Eng. 17 (2019) 1213–1225.

[94] E. Guibal, C. Roulph, P. Lecloirec, Uranium biosorption by a filamentous fungus Mucor miehei: pH effect on mechanisms and performances of uptake, Water Res. 26 (1992) 1139–1145.

[95] Y.S. Ho, G. McKay, Pseudo-second order model for sorption processes, Process Biochem. 34 (1999) 451–465.

[96] J. Crank, The Mathematics of Diffusion, 2nd. ed., Oxford University Press, Oxford, U.K., 1975, p. 414.

[97] J.-P. Simonin, On the comparison of pseudo-first order and pseudo-second order rate laws in the modeling of adsorption kinetics, Chem. Eng. J. 300 (2016) 254–263.

[98] M.A. Hubbe, S. Azizian, S. Douven, Implications of apparent pseudo-second-order adsorption kinetics onto cellulosic materials: A review, BioResources 14 (2019) 7582–7626.

[99] F.-X. Chen, C.-R. Zhou, G.-P. Li, F.-F. Peng, Thermodynamics and kinetics of glyphosate adsorption on resin D301, Arabian J. Chem. 9 (2016) S1665–S1669.

[100] J. Bai, F. Fan, X. Wu, W. Tian, L. Zhao, X. Yin, F. Fan, Z. Li, L. Tian, Y. Wang, et al., Equilibrium, kinetic and thermodynamic studies of uranium biosorption by calcium alginate beads, J. Environ. Radioact. 126 (2013) 226–231.

[101] S. Pérez-Conesa, J.M. Martínez, E. Sánchez Marcos, Hydration and diffusion mechanism of uranyl in montmorillonite clay: Molecular dynamics using an Ab Initio potential, J. Phys. Chem. C 121 (2017) 27437–27444.

[102] M.E. Mahmoud, M.F. Amira, A.A. Zaghloul, G.A.A. Ibrahim, High performance microwave-enforced solid phase extraction of heavy metals from aqueous solutions using magnetic iron oxide nanoparticles-protected-nanosilica, Sep. Purif. Technol. 163 (2016) 169–172.

[103] M.E. Mahmoud, G.M. Nabil, H. Abdel-Aal, N.A. Fekry, M.M. Osman, Imprinting "nano-SiO_2-crosslinked chitosan-nano-TiO_2" polymeric nanocomposite for selective and instantaneous microwave-assisted sorption of Hg(II) and Cu(II), ACS Sustainable Chem. Eng. 6 (2018) 4564–4573.

[104] R.G. Pearson, Acids and bases 151 (1966) 172–177.

[105] E.C. Lima, A. Hosseini-Bandegharaei, J.C. Moreno-Piráján, I. Anastopoulos, A critical review of the estimation of the thermodynamic parameters on adsorption equilibria. Wrong use of equilibrium constant in the Van't Hoof equation for calculation of thermodynamic parameters of adsorption, J. Mol. Liq. 273 (2019) 425–434.

[106] M. Ahmad, K. Yang, L. Li, Y. Fan, T. Shah, Q. Zhang, B. Zhang, Modified tubular carbon nanofibers for adsorption of uranium(VI) from water, ACS Appl. Nano Mater. 3 (2020) 6394–6405.

[107] E. Daneshvar, A. Vazirzadeh, A. Niazi, M. Kousha, M. Naushad, A. Bhatnagar, Desorption of methylene blue dye from brown macroalga: Effects of operating parameters, isotherm study and kinetic modeling, J. Cleaner Prod. 152 (2017) 443–453.

[108] D. Wu, A. Wang, L. Guo, Synthesis and application of Amberlite XAD-2 functionalized with dithizone for field preconcentration and separation of trace cadmium in seawater, Anal. Sci. 22 (2006) 1245–1248.

[109] Y.G. Yin, M. Chen, J.F. Peng, J.F. Liu, G.B. Jiang, Dithizone-functionalized solid phase extraction-displacement elution-high performance liquid chromatography-inductively coupled plasma mass spectrometry for mercury speciation in water samples, Talanta 81 (2010) 1788–1792.

[110] M. Truskolaska, K. Jankowski, Selective non-chromatographic determination of tributyltin in sediments using EDTA and diphenylcarbazone as masking agent, Int. J. Environ. Anal. Chem. 98 (2018) 295–307.

[111] K. Li, M. Li, D. Xue, Solution-phase electronegativity scale: Insight into the chemical behaviors of metal ions in solution, J. Phys. Chem. A 116 (2012) 4192–4198.

[112] I. Persson, Hydrated metal ions in aqueous solution: How regular are their structures? Pure Appl. Chem. 82 (2010) 1901–1917.

[113] M. Zhang, M. Yuan, M. Zhang, M. Wang, J. Chen, R. Li, L. Qiu, X. Feng, J. Hu, G. Wu, Efficient removal of uranium from diluted aqueous solution with hydroxypyridone functionalized polyethylene nonwoven fabrics, Radiat. Phys. Chem., 171 (2020) Art. N° 108742.

[114] G. Yuvaraja, M. Su, D.-Y. Chen, Y. Pang, L.-J. Kong, M.V. Subbaiah, J.-C. Wen, G. M. Reddy, Impregnation of magnetic - *Momordica charantia* leaf powder into chitosan for the removal of U(VI) from aqueous and polluted wastewater, Int. J. Biol. Macromol. 149 (2020) 127–139.

[115] S. Yu, J. Ma, Y. Shi, Z. Du, Y. Zhao, X. Tuo, Y. Leng, Uranium(VI) adsorption on montmorillonite colloid, J. Radioanal. Nucl. Chem. 324 (2020) 541–549.

[116] S. Saha, H. Basu, S. Rout, M.V. Pimple, R.K. Singhal, Nano-hydroxyapatite coated activated carbon impregnated alginate: A new hybrid sorbent for uranium removal from potable water, J. Environ. Chem. Eng., 8 (2020) Art. N° 103999.

[117] D. Ma, J. Wei, Y. Zhao, Y. Chen, S. Tang, The removal of uranium using novel temperature sensitive urea-formaldehyde resin: adsorption and fast regeneration, Sci. Total Environ., 735 (2020) Art. N° 139399.

[118] X. Liu, S. Hu, D. Xu, D. Shao, Removal of U(VI) from aqueous solution using carboxymethyl cellulose-modified Ca-rectorite hybrid composites, Korean J. Chem. Eng. 37 (2020) 776–783.

[119] L. Liang, X. Lin, Y. Liu, S. Sun, H. Chu, Y. Chen, D. Liu, X. Luo, J. Zhang, R. Shang, Carboxymethyl konjac glucomannan mechanically reinforcing gellan gum microspheres for uranium removal, Int. J. Biol. Macromol. 145 (2020) 535–546.

[120] N. Kolhe, S. Zinjarde, C. Acharya, Removal of uranium by immobilized biomass of a tropical marine yeast Yarrowia lipolytica, J. Environ. Radioact. 223–224 (2020) 106419.

[121] X. Hu, Y. Wang, J.O. Yang, Y. Li, P. Wu, H. Zhang, D. Yuan, Y. Liu, Z. Wu, Z. Liu, Synthesis of graphene oxide nanoribbons/chitosan composite membranes for the removal of uranium from aqueous solutions, Front. Chem. Sci. Eng. 14 (2020) 1029–1038.

[122] D.X. He, N. Tan, X.M. Luo, X.C. Yang, K. Ji, J.W. Han, C. Chen, Y.Q. Liu, Preparation, uranium (VI) absorption and reuseability of marine fungus mycelium modified by the bis-amidoxime-based groups, Radiochim. Acta 108 (2020) 37–49.

[123] M.F. Cheira, M.N. Kouraim, I.H. Zidan, W.S. Mohamed, T.F. Hassanein, Adsorption of U(VI) from sulfate solution using montmorillonite/polyamide and nano-titanium oxide/polyamide nanocomposites, J. Environ. Chem. Eng. 8 (2020). Art. N°104427.

[124] C. Chandra, F. Khan, Nano-scale zerovalent copper: green synthesis, characterization and efficient removal of uranium, J. Radioanal. Nucl. Chem. 324 (2020) 589–597.

[125] J. Bai, X. Ma, H. Yan, J. Zhu, K. Wang, J. Wang, A novel functional porous organic polymer for the removal of uranium from wastewater, Microporous Mesoporous Mater. 306 (2020). Art. N° 110441.

[126] P. Amesh, A.S. Suneesh, K.A. Venkatesan, M. Chandra, N.A. Ravindranath, High capacity amidic succinic acid functionalized mesoporous silica for the adsorption of uranium, Colloids Surf. A (2020) 602. Art. N° 125053.